REVISION 1

Title

FLUOROPHLOGOPITE FROM PIANO DELLE CONCAZZE (Mt. ETNA, ITALY): CRYSTAL CHEMISTRY AND IMPLICATIONS FOR THE CRYSTALLIZATION CONDITIONS

Authors

FERNANDO SCORDARI[1,*] • EMANUELA SCHINGARO[1] • GENNARO VENTRUTI[1] • EUGENIO NICOTRA[2] • MARCO VICCARO[2] • SIMONA MAZZIOTTI TAGLIANI[3]

Affiliation

[1]Dipartimento di Scienze della Terra e Geoambientali - Università degli Studi di Bari, Via E. Orabona 4, I-70125 Bari, Italy

[2]Dipartimento di Scienze Geologiche, Universita` di Catania, Corso Italia 57, I-95129 Catania, Italy

[3]Dipartimento di Scienze della Terra-Sapienza Università di Roma, Piazzale Aldo Moro 5, I-00185 Roma, Italy

[*]corresponding author:

Prof. F. Scordari

Dipartimento Geomineralogico, Università di Bari

Via Orabona 4, I-70125 Bari, Italy

e-mail: fernando.scordari@uniba.it

Abstract

In the present study, a full crystal chemical investigation of fluorophlogopite 1*M* from Piano delle Concazze, Mt. Etna volcano, Italy is carried out. The fluorophlogopite occurs in a benmoreitic lava from prehistoric volcanic activity at Mt. Etna (post-caldera forming phase of the "Ellittico" eruptive centre; ~15 ka BP). It is primarily associated with fluorapatite covered with amorphous SiO_2 and crystallized during syn/post-eruption pneumatolytic stages. The mica sample studied here is among the most Fe- and Ti-rich fluorophlogopite found in nature. EPMA data yielded the following mean chemical formula for this mineral:

$(K_{0.83}Na_{0.13})(Fe_{0.44}^{2+}Fe_{0.09}^{3+}Mg_{2.18}Al_{0.05}Ti_{0.23}Mn_{0.01})(Al_{0.92}Si_{3.08})O_{10.64}(Cl_{0.01}F_{1.35})$.

Structure refinements on four fluorophlogopite crystals, performed in space group *C*2/*m*, converged at R = 0.03-0.04, with cell parameters in the range a = 5.323–5.324, b = 9.219–9.222, c = 10.116–10.119 Å, β = 100.1–100.3°. Major substitutions are $OH^- \leftrightarrow F^-$, M^{3+}-oxy ($^{VI}M^{2+} + OH^- \leftrightarrow {}^{VI}M^{3+} + O^{2-}$) and Ti-oxy substitution: $^{VI}M^{2+} + 2(OH)^- \leftrightarrow {}^{VI}Ti^{4+} + 2O^{2-}$. The fluorophlogopite from Piano delle Concazze exhibits the shortest *c*-parameter with respect to other fluorophlogopites present in nature. The short *c* parameter is due essentially to the absence of the hydroxyl group in favor of F^- and expecially of O^{2-} and to the consequently increased attractive interaction between the interlayer cation and the anion content (F^-, O^{2-}) located at the O4 site. Other structural effects related to the peculiar composition of the anion site of the Piano delle Concazze fluorophlogopite are described in detail and discussed. A comparison with other natural fluorophlogopites (namely from Biancavilla, Etna and Presidente Olegario, Brazil) evidenced intermediate crystal chemical features for the Piano delle Concazze fluorophlogopite. Particularly at Etna, differences in the chemical composition of the crystallized fluorophlogopites could be related to various extent of enrichment by transfer of a gas phase achieved in distinct parts of the volcano plumbing system.

Keywords: Fluorophlogopite · Crystal chemistry · Substitution mechanisms · IR spectroscopy · Volatile transfer

INTRODUCTION

Fluorine-rich minerals are important indicators of the halogen activity in magmatic systems. From their investigation relevant inferences for the processes of magma differentiation acting in the shallow portions of the volcano plumbing system can be drawn. The intake of fluorine in micas is mainly governed by the temperature, the hydrofluoric acid activity during the crystallization and post-crystallization phase, the mica chemical composition and the entropy variation involved in the system mica-hydrothermal solution reaction (Boukili et al. 2002 and reference therein). Fluorine can be easily incorporated in trioctahedral micas as a substitute for hydroxyl at O4 anion site. The proton H^+ points almost directly toward the interlayer cation and, consequently, has a negligible interaction with the tetrahedral basal oxygens. The effects of F^- - OH^- substitution on the structure stability have attracted the attention of many researchers (Munoz 1984; Robert et al. 1993; Papin et al. 1997; Mason 1992; Boukili et al. 2001; Fechtelkord et al. 2003). The occurrences of F-rich natural micas are rare (Joswig 1972; Hazen and Burnham 1973; Russell and Guggenheim 1999) and a number of investigations concern synthetic fluorophlogopites (Takeda and Donnay 1966; McCauley et al. 1973; Takeda and Morosin 1975; Toraya et al. 1978, 1983), but also the studies on natural F-bearing micas carried out so far are in small number. However, recently, Gianfagna et al. (2007) performed a crystal structure analysis of the end-member F – bearing phlogopite from Biancavilla (Etna), that had been approved by the IMA-CNMMN as a new mineral with the name fluorophlogopite, whereas Brigatti et al. (2007) carried out a structural study of a fluorannite emphasizing the structural changes due to F content with respect to annite. Schingaro et al. (2011)

studying a variety of F- rich phlogopite from kamafugitic lavas of Presidente Olegario (Brazil) with the highest Ti content in nature and with a minor tetraferriphlogopite component, discuss the mechanisms of Ti and Fe incorporation in the phlogopite structure. On the other hand several phlogopites of volcanic origin with variable oxy component have been investigated recently (Schingaro et al. 2007; Matarrese et al. 2008; Scordari et al. 2010; Lacalamita et al. 2011) to understand how oxy substitutions affect the mica structure.

In the present work we aim at the full characterization of an oxy-fluorophlogopite with the maximum ($F^{-}+O^{2-}$) content (2 a.p.f.u.) found so far, occurring in benmoreitic lavas from the prehistoric volcanic activity of Mount Etna (~15 ka BP) (Nicotra et al. 2010). This mica is characterized by a F content (F = 1.35 a.pf.u.) intermediate between those from Biancavilla (F = 1.90 a.pf.u., Gianfagna et al. 2007) and the Ti-rich fluorophlogopite from Presidente Olegario (F = 0.90 a.pf.u., Schingaro et al. 2011). The main goal is to gain a deeper understanding of the structural effects caused in trioctahedral micas by F^{-} - OH^{-} substitution as well as by O^{2-} - OH^{-} via deprotonation associated with the intake of M^{3+}, Ti^{4+} on the octahedral layer. Another objective of this study is to investigate the relationship between the mineral phase rich in fluorine (fluorophlogopite) in some lavas erupted (15 ka) at Mt. Etna (Sicily, Italy) and the process active into the plumbing system. Due to the known substitutional complexity of micas, a combination of Electron probe microanalysis (EPMA), single-crystal X-ray diffraction (SCXRD) and Fourier Transform Infrared (FTIR) spectroscopy was used. The relationships between the physical and chemical crystallization conditions of such minerals, the role played by volatiles and some geochemical and volcanological aspects are discussed.

GEOCHEMICAL AND VOLCANOLOGICAL BACKGROUND

Mount Etna is a Quaternary composite volcano characterized by a within-plate magmatism (Viccaro and Cristofolini 2008 and references therein), which has grown up to its present elevation (< 3340

m a.s.l.) by accumulation of lavas and tephra throughout the last < 500 ka (Gillot et al. 1994). The first eruptive phases at Mt. Etna were characterized by the emission of tholeiitic pillow lavas and hyaloclastites together with transitional subaerial lavas (500-250 ka; Gillot et al. 1994). Most of the volcanic edifice is constituted, however, by Na-alkaline lavas and pyroclastics, emitted during the last 220 ka of activity at Etna (Romano 1982; Branca et al. 2008; Ferlito and Nicotra 2010; Nicotra et al. 2011; Viccaro et al. 2011 and references therein). The relevant volcano-stratigraphic succession is divided into four major phases (Monaco et al. 2011 and references therein), namely: 1) Timpe volcanics (220-100 ka); 2) Valle del Bove volcanics (100-60 ka); 3) Ellittico (60-15 ka) and 4) Recent Mongibello (15 ka to present). Fluorophlogopite crystals studied in this work were found by Nicotra et al. (2010) in a benmoreitic lava (EL85 sample) that belongs to the Ellittico volcanic centre. The EL85 lava flow has a thickness of 2 m and lies at the base of a 40-m-thick sub-horizontal volcanic sequence in the Piano delle Concazze area (~2790 m a.s.l.; Fig. 1). The EL85 benmoreite, which is one the most differentiated of the entire Etnean volcanic succession (Corsaro and Cristofolini 1996; Viccaro and Cristofolini 2008; Nicotra et al. 2010; Nicotra et al. 2011), is characterized by the occurrence of fluorine-rich phases such as fluorophlogopite (grown within lava vesicles) and fluorapatite. Apart from these peculiar accessory phases, phenocrysts of the EL85 volcanic rock are those of the classical mineralogical assemblages at Etna, namely: plagioclase (~10 vol.%), augitic clinopyroxene (~5 vol.%), Fo_{57-69} olivine (~2 vol.%), titaniferous magnetite (~2 vol.%). Simulations of crystal fractionation demonstrated that the EL85 compositions have anomalous enrichments in some major and trace elements (e.g., Ti, Fe, K, Ba and, to a minor extent, Rb and REEs). Furthermore, chlorine and fluorine concentrations (0.20 wt.% and 0.34 wt.% respectively) are significantly higher than those of other Etnean prehistoric mugearites and benmoreites. This selective enrichment was interpreted by Nicotra et al. (2010) as due to flushing of volatiles released by more primitive and volatile-rich magmas during their ascent towards shallower levels of the feeding system.

In the present work, four crystals of fluorophlogopite from EL85 were selected to be investigated using multiple analytical approach.

EXPERIMENTAL

CHEMICAL COMPOSITION

EPMA data of the same crystals used for crystal structure refinement were obtained with a Cameca SX-50 apparatus installed at Istituto di Geologia Ambientale e Geoingegneria (IGAG), Università di Roma "La Sapienza". The analyses were performed in wavelength-dispersive spectroscopic (WDS) mode with a 15 kV accelerating voltage, 15 nA beam current and a 10 μm beam-spot size. The following standards were employed: jadeite (Na), periclase (Mg), wollastonite (Si and Ca), rutile (Ti), corundum (Al), magnetite (Fe), orthoclase (K), barite (Ba), fluorophlogopite (F), sylvite (Cl). Conversion from X-ray counts to oxide weight percentages (wt%) was obtained with the PAP data reduction method (Pouchou and Pichoir 1985). Chemical composition results (Table 1), obtained from at least eight-point analyses, show that the samples examined are relatively homogeneous, particularly regarding Al_2O_3 (11.0–11.2 wt%), MgO (19.5–20.1 wt%), FeO (8.1–9.1 wt%), TiO_2(3.9–4.3 wt%), K_2O (8.5–9.1 wt%), Na_2O (0.7–1.1 wt%), and fluorine (5.5–6.0 wt%) contents, in agreement with previous chemical determinations (Nicotra et al. 2010).

INFRARED SPECTROSCOPY

Room temperature FTIR measurements were carried out by means of a Nicolet Avatar FTIR spectrometer, equipped with a Continuum microscope, a MCT nitrogen-cooled detector and a KBr beam splitter. Unpolarized spectra have been acquired in transmission mode on flakes of single crystals mounted on glass capillaries and oriented with the (001) cleavage plane normal to the incident infrared radiation. Final spectrum was collected in the 4000-1400 cm^{-1} range by co-adding 128 scans with a 4 cm^{-1} nominal resolution.

SINGLE-CRYSTAL X-RAY DIFFRACTION

Four selected crystals (labeled E0, E1, E2, E3 samples) were examined by single-crystal diffraction at room temperature using a Bruker AXS APEX2 diffractometer equipped with a CCD detector and graphite-monochromatized Mo*K*α radiation (λ = 0.71073 Å). Operating conditions were: 50 kV, 30 mA. For each measurement, three sets of 12 frames were acquired with 0.5° φ rotation and the results were used for the initial unit-cell determinations. The collection strategy was optimized by the Apex program suite (Bruker 2008a); the intensities of reflections in the entire Ewald sphere (±*h*, ±*k*, ±*l*) were recorded by a combination of ω and φ rotation sets with a 0.5° scan width and exposure times from 10 to 30 s/frame. Only one (E2) out of the four crystals selected for data collection resulted to be a simple 1*M* polytype, whereas the remaining three were found to be 1*M* polytypes twinned by pseudo-merohedry, each twin being composed of three individual components rotated by ±120° around c*. In the latter case, the orientation matrices of the three components were identified using the program Cell_Now (Bruker. 2008b) and the relevant twin laws employed in the structure refinement. The package SAINT-IRIX (Bruker 2008a) was used for data reduction, including intensity integration; the data were corrected for Lorentz-polarization, background effects and scale variation. The final unit-cell parameters were obtained from the *xyz* centroids of the measured reflections after integration and are reported in Table 1, together with details on data collection. A semi-empirical absorption correction based on the determination of transmission factors for equivalent reflections (Blessing 1995) was applied using TWINABS software (Bruker 2008a).

The structure refinements were performed in space group *C*2/*m* using program CRYSTALS (Betteridge et al. 2003) starting from the atomic parameters in Scordari et al. (2006). Scattering curves for fully ionized chemical species were used for non-tetrahedral sites, whereas ionized *vs.* neutral scattering curves were employed for Si and O (Hawthorne et al. 1995). Reflections with $I > 3\sigma(I)$ were used for the structure refinements. Refined parameters were: atomic positions, cations

occupancies, anisotropic atomic displacement parameters, overall scale factor and, whenever appropriate, twin component scale factors. The latter refined to the following values : 0.861, 0.138, 0.001 for sample E0; 0.983, 0.016, 0.001 for sample E1; 0.521, 0.467, 0.012 for sample E3. Accordingly, only sample E3 consisted of two twin components of comparable volume, whereas samples E0 can be described by one predominant twin component one subordinate in volume and E1 has only one predominant twin component. For each crystal the calculated difference-Fourier maps revealed no significant excess in electron density above the background. The slight asymmetry in $\Delta\rho_{min}$ - $\Delta\rho_{max}$ values for E0 and E1 samples are likely due to the not optimal modeling of the subordinate twin component. The relevant details of each structure refinement are reported in Table 2. Final atomic coordinates, site occupancies and anisotropic and equivalent isotropic displacement parameters are given in Table 3. Selected bond distances are listed in Table 4, whereas the distortion parameters for micas are reported in Table 5. Mean atomic numbers and octahedral and tetrahedral bond distances are compared to those calculated from chemical analyses using radii from Shannon (1976) and mean anion radii from Kogarko et al. (2005) in Table 6.

RESULTS AND DISCUSSION

Chemical features

The structural formula calculation can be complicated by the concomitant presence of elements with variable valence state (Fe, Ti) and possible occurrence of vacancies in the structure sites (Waters and Charnley 2002; Mesto et al. 2006; Scordari et al. 2008). The crystal-chemical formulas for the refined crystals shown in Table 1 were obtained by combining EPMA data and results of the structure refinement. The formulas were calculated on the basis of 12 (O, OH, F, Cl) total anions and assuming all Ti as Ti^{4+}. The H_2O content was set zero according to the indication from the IR

spectrum (Fig. 2), which did not show any typical OH-stretching absorption band near 3700 cm^{-1} (as shown in the inset from a biotite studied by Scordari et al., 2006).

The Fe^{2+}/Fe^{3+} ratio was varied to obtain a good agreement between X-ref and EPMA derived mean atomic numbers, as well as between <M-O> observed and calculated distances from ionic radii of Shannon (1976).

The above considerations as well as charge balance requirements lead to the following average structural formula $(K_{0.83}Na_{0.13})(Fe_{0.44}^{2+}Fe_{0.09}^{3+}Mg_{2.18}Al_{0.05}Ti_{0.23}Mn_{0.01})(Al_{0.92}Si_{3.08})O_{10.64}(Cl_{0.01}F_{1.35})$. The latter formula as well as those reported in Table 1 evidence that in the analyzed crystals, the tetrahedral site is occupied by Si and Al in a ratio Si/(Si+Al) ~ 0.77, the octahedral sites are mainly occupied by Mg, Fe and Ti with minor amounts of Al and Mn, and the interlayer site is almost full, with K as dominant cation, minor Na, and negligible Ba (kinoshitalite component) and vacancy (~0.04 a.p.f.u.) content. The other notable chemical features of the studied samples are the high F content, almost constant around 1.35 a.p.f.u and the appreciable O^{2-} content (on average 0.64 a.p.f.u.) that saturate the anionic site. With respect to fluorophlogopite from Biancavilla (Gianfagna et al. 2007) the Piano delle Concazze samples have lower F content and higher Ti and Fe contents, whereas if compared to Presidente Olegario micas (Schingaro et al. 2011) the same samples are oxy-fluorophlogopites with the highest Fe content investigated to date (e.g., Gianfagna et al. 2007 and references therein). The main substitutions in the studied micas are: fluorine hydroxyl substitution [$OH^- \leftrightarrow F^-$], Ti-oxy substitution [$^{VI}M^{2+} + 2(OH)^- \leftrightarrow {}^{VI}Ti^{4+} + 2(O^{2-})$], with minor M^{3+}-oxy substitution.

Structural features

The cell parameters (Table 2), bond distances (Table 4) and the main structural features (Table 5) of the crystals investigated here display small variations, consistently with the chemical homogeneity of the sample analyzed (see Table 1). In particular, our fluorophlogopite sample is characterized by

the smallest *c* parameter (see Fig. 3) recorded to date (Gianfagna et al. 2007, Brigatti and Guggenheim 2002). Neglecting the effect of the mean interlayer radius (see below), the reduction of the *c* parameter can be ascribed essentially to two different substitution mechanisms both of which, in different ways, change the H^+-K^+ coulombic repulsion into the electrostatic attractive interaction between the interlayer cation and the O4 anionic site: 1) the entrance of F in the mica structure through the $OH^- \leftrightarrow F^-$ substitution; 2) the oxygen deprotonation at the O4 anionic site through $M^{3+,4+}$-oxy substitutions mechanism, (Cesare et al. 2003; Scordari et al. 2006 and references therein). The decrease of *c* parameter in phlogopites upon loss of H^+ is well-documented in literature (Redhammer et al., 2005; Ventruti et al., 2008). The structural effects of the two above substitutions cannot be easily solved, since usually they superimpose or enhance each other. Figure 3 shows the variation of *c* parameter as a function of the $F^- + O^{2-}$ content. All the selected samples plot in an area delimited by two straight lines: one relevant to the join end member phlogopite (Redhammer and Roth 2002) - end member fluorophlogopite (Takeda and Morosin 1975), the other to the join end member phlogopite (Redhammer et al. 2005) - oxyphlogopite (Cesare et al. 2003). Note that the slope of the latter is steeper than that of the former due to increased K^+-O^{2-} attraction with respect to the K^+-F^- one. We observe that: a) the investigated sample (F^-= 1.35 a.p.f.u.; O^{2-}= 0.64 a.p.f.u.) has shorter *c* parameter with respect to Biancavilla sample (F^-= 1.90 a.p.f.u.; O^{2-}= 0.00 a.p.f.u.) due to the enhanced attractive effect of the oxy component; b) compared to Hazen and Burhnam (1973) sample (F^-= 1.30 a.p.f.u.; O^{2-}= 0.00 a.p.f.u.), which has almost the same F content as Concazze fluorophlogopite, the further contraction of the *c* parameter may be ascribed to the oxy component which is missing or negligible in Hazen and Burhnam (1973) sample; c) compared to sample SA (F^-= 0.10 a.p.f.u.; O^{2-}= 0.62 a.p.f.u.) which has the same oxy concentration as our sample but low F content, the extra shortening detected in Concazze fluorophlogopite is the result of the increased F content.

We also observe that the shortening effect caused by the oxy-substitution is not linear in the whole *c*-range. Indeed the comparison of the samples SA and HO20 ((F^-= 0.00 a.p.f.u.; O^{2-}= 0.71 a.p.f.u.) - at high *c* values in the figure - shows that, in spite of the similarity of the $F^- + O^{2-}$ content (ΔO^{2-}= 0.09 a.p.f.u,) the slight difference in the oxy component leads to a strong reduction of the *c* parameter (Δc = 0.05Å). On the other hand considering the sample from Takeda and Morosin 1975 (F^-= 2.00 a.p.f.u.; O^{2-}= 0.00 a.p.f.u.) and from Concazze ((F^-= 1.35 a.p.f.u.; O^{2-}= 0.65 a.p.f.u., this work) - at low *c* values in the figure - it is apparent that a large difference in the oxy component(ΔO^{2-}= 0.65 a.p.f.u.) results in a much smaller reduction of the *c* parameter (Δc = 0.02Å) than the previous case.

The relationship $c \sin(\beta) = 2\ t_{tet} + t_{oct} + t_{int}$ allows to discriminate the contribution of each sheet thickness on the whole *c* cell parameter. The reduction of the *c* cell parameter is mainly related to the shrinking of the interlayer thickness as illustrated in Figure 4. The effects of the F^-+O^{2-} substitutions are better described in this figure, where the sample distribution is slightly different from that in Figure 3. This is due to the fact that the contribution of octahedral and tetrahedral sheets is missing. From the inspection of the Figure 4 the interlayer separation decreases from 3.32 Å and 3.30 Å, respectively in Biancavilla fluorophlogopite (Gianfagna et al. 2007) and Olegario fluorophlogopite (Schingaro et al. 2011) to about 3.29 Å in our samples. On the other hand tetrahedral thickness remains unchanged (2.24 Å) and octahedral thickness slightly increases from 2.11 Å in Biancavilla fluorophlogopite (Gianfagna et al. 2007) to 2.12 Å in Olegario fluorophlogopite (Schingaro et al. 2011) and in Piano delle Concazze fluorophlogopite of this study. The latter effect reflects octahedral heterovalent substitutions, particularly those relevant to Fe and Ti contents. The *a* and *b* cell parameters resulted to be intermediate between those corresponding to Biancavilla fluorophlogopite and Olegario fluorophlogopite but closer to the latter in agreement with the presence of similar heterovalent substitutions. A detailed comparison of selected structural features of fluorophlogopite from Biancavilla and Olegario is given in Table 7. In Piano delle

Concazze fluorophlogopite, the tetrahedron is fairly regular for all the four analyzed crystals with tetrahedral bond lengths T-O and the tetrahedral volume very close, within one standard deviation (Tables 4, 5), to the corresponding values found for the fluorophlogopite from Biancavilla (Gianfagna et al. 2007). This is due to the very similar composition of tetrahedral site (Si/(Si+Al) = 0.8) of the Biancavilla sample. The slight stretching of the tetrahedra along the T-O apical bond distance (O_{basal}-T-O_{apical}≈ 110.7°, O_{basal}-T-O_{basal}= 108.23°) of the Piano delle Concazze samples compared to that published in Brigatti and Guggenheim (2002) is also related to the high Si content. The tetrahedral sheet adapts its lateral dimension along the *a* and *b* axes through mutual rotation of the individual tetrahedra to compensate for the misfit with the octahedral sheet size (Mercier et al. 2005). This misfit, known as the in-plane rotation angle (α), is mainly a function of octahedral sheet compositions and secondarily of tetrahedral sheet composition, and is the most effective mechanism to obtain congruence between tetrahedral and octahedral sheet sizes in micas. The Piano delle Concazze fluorophlogopite of this study showed a small in-plane rotation angle (α= 4.8°), which is similar to other natural fluorophlogopites and synthetic counterparts (e.g., Gianfagna et al. 2007). Taking into account that the fluorophlogopite from Piano Concazze and fluorophlogopite from Biancavilla are characterized by same tetrahedral site size, the lower value of ditrigonal angle α in our sample is due to a increased lateral dimension of octahedral sheet. In addition to the in-plane rotation angle, α, the tetrahedral sheet corrugation (Δz) also reflects the slight tetrahedral-octahedral layers mismatching. In regular tetrahedra, this corrugation is accomplished by cooperative tetrahedral tilting due to adjustments of the z-coordinates of the O1 basal oxygens, keeping the O2 atoms fixed (Mercier et al. 2005). This parameter was observed to decrease with increasing F content (Brigatti et al. 2007). More generally, the basal corrugation parameter is also related to the geometric meso-octahedral character (Brigatti and Guggenheim 2002). This is the case of Concazze phlogopite, which displays average <M1-O> distances systematically larger than the <M2-O> distances (see Table 4) resulting meso-octahedral from a geometric view (Weiss et al. 1985, 1992).

Although the differences (see Table 6) in the refined mean atomic numbers (m.a.n.) between M1 and M2 site (see below) suggest that the samples here analyzed are chemically homo-octahedral (Ďurovič 1994; Ferraris and Ivaldi 2002; Nespolo and Ďurovič 2002), the inspection of octahedral distortion parameters (individual mean bond distances, flattening angles and off-center shift of the M2 site, Tables 4 and 5) point to some degree of chemical ordering into octahedral sites. Specifically the H deficiency and the cationic displacement from the geometric center of the M2 octahedra (Table 5) are clear clues for the occurrence of oxy type substitution mechanisms. This results in the alteration of a number of structural parameters that, in turn, are employed to identify the occurrence of $M^{3+,4+}$-oxy substitution mechanisms (Schingaro et al. 2005, 2007; Scordari et al. 2006, 2008, 2010; Cesare et al. 2008; Matarrese et al. 2008; Ventruti et al. 2008).

In particular, Fig. 5 shows a good correlation between the off-center shift *vs*. Ti content. The Ti-oxy substitution implies the full partitioning of Ti into the M2 site. The most likely cation partition that can be derived from the above considerations and from the average chemical composition is: $Mg_{0.70}Fe^{2+}_{0.23}Fe^{3+}_{0.01}Al_{0.05}Mn_{0.01}$ for the M1 site, (m.a.n. = 15.54 e^-; <M1-O>=2.075), and $Mg_{0.74}Fe^{2+}_{0.095}Fe^{3+}_{0.05}Ti_{0.115}$ for the M2 site (m.a.n. = 15.18 e^-; <M2-O>=2.059).

Other effects associated with the deprotonation of the O4 anion sites are: a depression of the O4 oxygen that is responsible for the non coplanarity of the O4 anionic site with the O3 tetrahedral apical oxygen atom; the decrease of the O4-O4 distance to provide a better screening to the increased positive charge between adjacent M2 sites (Ventruti et al. 2008).

This effect is further enhanced by the F^- - OH^- replacement in our sample, as also illustrated in Figs. 3 and 4 above. In Fig.6 a clear correlation is apparent between O4-O4 shortening and the increase of the (O^{2-}, F^-) content at the anionic site.

Finally, a more regular arrangement of the interlayer site is also observed as a consequence of an increase of the shorter cation-oxygen distances $<K\text{-}O>_{inner}$ and a concomitant decrease of the longer ones, $<K\text{-}O>_{outer}$, that is consistent with the small value of the ditrigonal rotation angle α.

The small value of ΔK-O (Table 5) is directly related to the tetrahedral site volume (Fig.7). This effect is due to the increase of the Si content and the consequent decrease of the tetrahedral bond distances that provide a greater bond valence contribution to the charge balance of the basal oxygen atoms, thus stabilizing the structure. Finally Hawthorne et al. (1999) showed that a monotonic correlation occurs between the *c* parameter and the mean interlayer radius. Actually their correlation does not take into account structural distortion due to the interaction between interlayer and O4 sites. In our sample, the mean interlayer cation radius results into a *c* value considerably smaller than that expected from the analysis in Hawthorne et al.1999 (see Fig. 8). This is due to the fact that the structural effects caused by the F^{-} - OH^{-} substitution are enhanced by the concomitant occurrence of the OH^{-} group deprotonation.

All the observed trends confirm the strong influence of anionic site on the overall unit layer topology of the examined fluorophlogopite sample, with particular reference to the structural features measured along the K-O4 direction.

PETROLOGICAL AND VOLCANOLOGICAL IMPLICATIONS

The fluorophlogopite found in the Piano delle Concazze lavas differs from the fluorophlogopite of the Biancavilla lavas mainly for the higher Fe and Ti and lower OH^{-} and F^{-}. These compositional differences should reflect distinct physical-chemical conditions at the time of crystallization, in relation primarily to the amount of available volatiles into the feeding system. As noted by some authors (Nicotra et al. 2010; Mazziotti-Tagliani et al. 2012), the occurrence of the F-rich mineralogical phases (particularly fluorophlogopite) is attributed to volatile flushing of a resident magma reservoir. This mechanism can produce selective transfer of some elements that are carried by a gas phase, finally leading to anomalous concentrations of elements with great affinity with fluids or that can be complexed (Rittmann 1962; Caroff et al.1997; Greenough et al. 1999; de Hoog and Van Bergen 2000; Ferlito et al. 2008; Nicotra et al. 2010). Experimental results confirm the

346 combined action of water and halogens in complexing and carrying elements such as Fe, Ti, K, P in
347 magmatic systems (Frank et al. 2003; Stelling et al. 2008). The consequent influx of a gas phase
348 enriched in metal-halogen-complexes into a volatile-undersaturated magma may then be viewed as
349 the process leading to selective enrichments in some elements, and particularly halogens, in the
350 residing magma.
351 In such a picture, differences in the chemical composition of the fluorophlogopites crystallized in
352 products emitted at Piano delle Concazze and Biancavilla could be ascribed to variable degrees of
353 differentiation induced by volatile transfer that was attained in distinct zones of the plumbing
354 system. In this regard, the geometry of the Etnean plumbing system is thought to be constituted by a
355 dense network of dykes and sills in the central portions (corresponding to the main open-conduit
356 system), which can also coalesce to form shallow magma reservoirs (Ferlito and Nicotra 2010;
357 Nicotra and Viccaro 2012). By contrast, peripheral zones of the volcano plumbing system are more
358 tectonically-controlled, and minor magma intrusion occur. Thus, magma ascent and degassing
359 dynamics in the central conduit and peripheral portions of the edifice are expected to be
360 significantly different. A reason for the higher Fe and Ti and lower OH^- and F^- in the Piano delle
361 Concazze fluorophlogopite (open-conduit system) than in the Biancavilla crystals (peripheral closed
362 system) could be found in a more efficient gas flushing that took part into the central portion of the
363 plumbing system. Furthermore, the lower amount of OH^- and F^- of fluorophlogopite crystals of
364 Piano delle Concazze could be indication that these lavas experienced, before the eruption, very
365 shallow degassing in the summit portion of the central conduit (<10 MPa, i.e. the exsolution
366 pressure of fluorine in basaltic magmas at Mt. Etna; see Alletti et al. 2009). Conversely, the
367 peripheral closed system erupting at Biancavilla did not allow marked degassing, and the formed
368 gas phase at depth was kept in contact with the magma until the eruption. This leads to a high
369 concentration of H_2O and F in the system, and great availability of OH^- and F^- during the later
370 syn/post eruptive stages of crystallization.

ACKNOWLEDGEMENTS

Financial support was provided by COFIN MIUR. The authors thank the Technical Editor, the Associated Editor R. Yuretich, G. Redhammer and one anonymous reviewer for their constructive comments to this manuscript.

REFERENCES CITED

Alletti, M., Baker D.R., Scaillet, B., Aiuppa, A., Moretti, R., Ottolini, L. (2009) Chlorine partitioning between a basaltic melt and H_2O-CO_2 fluids at Mount Etna. Chemical Geology, 263, 37-50.

Betteridge, P.W., Carruthers, J.R., Cooper, R.I., Prout, K., and Watkin, D.J. (2003) Crystals version 12: software for guided crystal structure analysis. Journal of Applied Crystallography, 36, 1487.

Blessing, R.H. (1995) An empirical correction for absorption anisotropy. Acta Crystallographica A, 51, 33-38.

Boukili, B., Robert, J.-L., Beny, J.M., and Holtz, F. (2001) Structural effects of OH → F substitution in trioctahedral micas of the system: K_2O-FeO-Fe_2O_3-Al_2O_3-SiO_2-H_2O-HF. Schweizerische Mineralogische und Petrographische Mitteilungen, 81, 55–67.

Boukili, B., Holtz, F., Bény, J.M., and Robert, J.L. (2002) Fe-F and Al-F avoidance rule in ferrous-aluminous (OH,F) biotites. Schweizerische Mineralogische und Petrographische Mitteilungen, 82, 549–559.

Branca S., Coltelli M., De Beni E., Wijbrans J. (2008). Geological evolution of Mount Etna volcano (Italy) from earliest products until the first central volcanism (between 500 and 100 ka ago)

inferred from geochronological and stratigraphic data. International Journal of Earth Science, 97:135–152.

Brigatti, M.F. and Guggenheim, S. (2002) Mica crystal chemistry and the influence of pressure, temperature, and solid solution on atomistic models. In A. Mottana, F.P. Sassi, J.B. Thompson Jr., and S. Guggenheim, Eds., Micas: Crystal Chemistry and Metamorphic Petrology, 46, p. 1–97. Reviews in Mineralogy and Geochemistry, Mineralogical Society of America and the Geochemical Society, Chantilly, Virginia.

Brigatti, M.F., Caprilli, E., Malferrari, D., and Mottana, A. (2007) Crystal structure and crystal chemistry of fluorannite and its relationships to annite. Mineralogical Magazine, 71, 683–690.

Bruker (2008a). *APEX2*, *SAINT* and *TWINABS*. Bruker AXS Inc., Madison, Wisconsin, USA

――― (2008b). *Cell Now*. Bruker AXS Inc., Madison, Wisconsin, USA.

Caroff, M., Ambrics, C., Maury, R.C., Cotton, J. (1997) From alkali basalt to phonolite in hand-size samples: vapor-differentiated effects in the Bouzentes lava flow (Cantal, France). Journal of Volcanology and Geothermal Research, 79, 47-61.

Cesare, B., Cruciani, G., and Russo, U. (2003) Hydrogen deficiency in Ti-rich biotite from anatectic metapelites (El Joyazo, SE Spain): Crystal-chemical aspects and implications for high-temperature petrogenesis. American Mineralogist, 88, 583–595.

Cesare, B., Satish-Kumar, M., Cruciani, G., Pocker, S., and Nodari, L. (2008) Mineral chemistry of Ti-rich biotite from pegmatite and metapelitic granulites of the Kerala Khondalite Belt (southeast India): Petrology and further insight into titanium substitutions. American Mineralogist, 93, 327–338.

Corsaro, RA, and Cristofolini, R. (1996) Origin and differentiation of recent basaltic magmas from Mount Etna, Mineralogy and Petrology, 57, 1-21.

de Hoog, J.C.M., van Bergen, M.J. (2000) Volatile-induced transport of HFSE, REE, Th and U in arc magmas: evidence from zirconolite-bearing vesicles in potassic lava of Lewotolo volcano (Indonesia). Contribution to Mineralogy and Petrology, 139, 485-502.

Donnay, G., Morimoto, N., Takeda, H., and Donnay, J.D.H. (1964a) Trioctahedral one-layer micas. I. Crystal structure of a synthetic iron mica. Acta Crystallographica, 17, 1369–1373.

Donnay, G., Donnay, J.D.H., and Takeda, H. (1964b) Trioctahedral one-layer micas. II. Prediction of the structure from composition and cell dimensions. Acta Crystallographica, 17, 1374–1381.

Ďurovíč, S. (1994) Classification of phyllosilicates according to the symmetry of their octahedral sheets. Ceramics, Silikáty, 38, 81–84.

Fechtelkord, M., Behrens, H., Holtz, F., Bretherton, J.L., Fyfe, C.A., Groat, L.A., and Raudsepp, M. (2003) Influence of F content on the composition of Al-rich synthetic phlogopite: Part II. Probing the structural arrangement of aluminum in tetrahedral and octahedral layers by 27Al MQMAS and 1H/19F-27Al HETCOR and REDOR experiments. American Mineralogist, 88, 1046–1054.

Ferlito C. and Nicotra E. (2010). The dykes swarm of Mount Calanna (Etna, Italy): an example of the uppermost portion of a volcanic plumbing system. Bulletin of Volcanology 72, 1191-1207.

Ferlito, C., Viccaro, M., Cristofolini, R. (2008) Volatile-induced differentiation in the plumbing system of Mt. Etna volcano (Italy): evidence from glass and tephra of the 2001 eruption. Bulletin of Volcanology, 70, 455-473.

Ferraris, G. and Ivaldi, G. (2002) Structural features of micas. In A. Mottana, F.P. Sassi, J.B. Thompson Jr., and S. Guggenheim, Eds., Micas: Crystal Chemistry and Metamorphic Petrology, 46, p. 117–153. Reviews in Mineralogy and Geochemistry, Mineralogical Society of America and the Geochemical Society, Chantilly, Virginia.

Foley, S.F. (1989) Experimental constraints of phlogopite chemistry in lamproites; 1, The effect of water activity and oxygen fugacity. European Journal of Mineralogy, 1, 411–426.

Foley, S.F., Venturelli, G., Green, D.H., and Toscani, L. (1987) The ultrapotassic rocks: Characteristics, classification and constraints for petrogenetic models. Earth Science Reviews, 24, 81–134.

Frank, M.R., Candela, P.A. Piccoli, P.M. (2003) Alkali exchange equilibria between a silicate melt and coexisting magmatic volatile phase: an experimental study at 800°C and 100 MPa. Geochimica et Cosmochimica Acta,67, 1415-1427.

Gianfagna, A., Scordari, F., Mazziotti-Tagliani, S., Ventruti, G., and Ottolini, L. (2007) Fluorophlogopite from Biancavilla (Mt. Etna, Sicily, Italy): Crystal structure and crystal chemistry of a new F-dominant analog of phlogopite. American Mineralogist, 92, 1601–1609.

Gianfagna A, Oberti R (2001) Fluoro-edenite from Biancavilla (Catania, Sicily, Italy): crystal chemistry of a new amphibole end-member. American Mineralogist 83,1486-1493.

Gillot, P.Y., Kieffer, G., Romano, R. (1994): The evolution of Mount Etna in the light of potassium-argon dating. Acta Vulcanologica, 5, 81–87.

Greenough, J.D., Lee, C.Y., Fryer, B.J. (1999) Evidence for volatile influenced differentiation in a layered alkali basalt flow, Penghu Island, Taiwan. Bulletin of Volcanology, 60, 412-424.

Hawthorne, F.C., Ungaretti, L., and Oberti, R. (1995) Site populations in minerals: terminology and presentation of results. Canadian Mineralogist, 33, 907–911.

Hawthorne, F.C., Teertstra, D.K. and Černý, P. (1999) Crystal-structure refinement of a rubidian cesian phlogopite. American Mineralogist, 84, 778–781

Hazen, R.M. and Burnham, C.W. (1973) The crystal structures of one-layer phlogopite and annite. American Mineralogist, 58, 889–900.

Joswig, V.W. (1972) Neutronenbeugungsmessungen an einem 1M-phlogopit. Neues Jahrbuch für Mineralogie, Monatshefte, 1–11.

Kogarko, L.N., Uvarova, Y.A., Sokolova, E., Hawthorne, F.C., Ottolini, L., and Grice, J.D. (2005) Oxykinoshitalite, a new mica from Fernando-de-Norohna Island, Brazil: occurrence and crystal structure. Canadian Mineralogist, 43, 1501-1510.

Lacalamita, M., Schingaro, E., Scordari, F., Ventruti, G., Fabbrizio, A., Pedrazzi, G. (2011). Substitution mechanisms and implications for the estimate of water fugacity for Ti-rich phlogopite from Mt. Vulture, Potenza, Italy. American Mineralogist, 96, 1381-1391.

Mason, R.A. (1992) Models of order and iron-fluorine avoidance in biotite. Canadian Mineralogist, 30, 343–354.

Matarrese, S., Schingaro, E., Scordari, F., Stoppa, F., Rosatelli, G., Pedrazzi, G., and Ottolini, L. (2008) Crystal chemistry of phlogopite from Vulture-S. Michele Subsynthem volcanic rocks (Mt. Vulture, Italy) and volcanological implications. American Mineralogist, 93, 426-437.

Mazziotti Tagliani S, Angelone M, Armiento G, Pacifico R, Cremisini C, Gianfagna A (2012) Arsenic and fluorine in the Etnean volcanics from Biancavilla, Sicily, Italy: environmental implications. Environmental Earth Science, 66, 561-572.

Mazziotti Tagliani, S., Nicotra, E., Viccaro, M., Gianfagna, A. (2012) Halogen-dominant mineralization at Mt. Calvario dome (Mt. Etna) as a response of volatile flushing into the magma plumbing system. Mineralogy and Petrology, 106, 89-105.

McCauley, J.W., Newnham, R.E., and Gibbs, G.V. (1973) Crystal structure analysis of synthetic fluorophlogopite. American Mineralogist, 58, 249–254.

Mercier, P.H.J., Evans, R.G., and Rancourt, D.G. (2005) Geometric crystal chemical models for structural analysis of micas and their stacking polytypes. American Mineralogist, 90, 382–398.

Mesto, E., Schingaro, E., Scordari, F., and Ottolini, L. (2006) An electron microprobe analysis, secondary ion mass spectrometry, and single crystal X-ray diffraction study of phlogopites from Mt. Vulture, Potenza, Italy: Consideration of cation partitioning. American Mineralogist, 91, 182–190

Monaco, C., De Guidi, G., Ferlito, C. (2011) The morphotectonic map of Mt. Etna. Italian Journal of Geosciences, 129, 408-428.

Munoz, J.L. (1984) F-OH and Cl-OH exchange in micas with application to hydrothermal deposits. In S.W. Bailey, Ed., Micas, 13, p. 469–493. Reviews in Mineralogy, Mineralogical Society of America, Chantilly, Virginia.

Nespolo, M. and Ďurovič, S. (2002) Crystallographic basis of polytypism and twinning in micas. In A. Mottana, F.P. Sassi, J.B. Thompson Jr., and S. Guggenheim, Eds., Micas: Crystal Chemistry and Metamorphic Petrology, 46, p. 155–279. Reviews in Mineralogy and Geochemistry, Mineralogical Society of America and the Geochemical Society, Chantilly, Virginia.

Nicotra, E., Viccaro, M., (2012) Unusual magma storage conditions at Mt. Etna (Southern Italy) as evidenced by plagioclase megacryst-bearing lavas: implications for the plumbing system geometry and summit caldera collapse. Bulletin of Volcanology, doi:10.1007/s00445-011-0566-9.

Nicotra E., Viccaro M., Ferlito C., Cristofolini R. (2010). Influx of volatiles into shallow reservoirs at Mt. Etna volcano (Italy) responsible for halogen-rich magmas. European Journal of Mineralogy 22, 121-138.

Nicotra, E., Ferlito, C., Viccaro, M., Cristofolini, R. (2011) Volcanic geology and petrology of the Val Calanna succession(Mt. Etna, Southern Italy): discovery of a new eruptive center. Periodico di Mineralogia, 80, 287-307.

Papin, A., Sergent, J., and Robert, J-L. (1997) Intersite OH-F distribution in an Al-rich phlogopite. European Journal of Mineralogy, 9, 501–508.

Pouchou, J.L. and Pichoir, F. (1985) "PAP" Φ(ρZ) procedure for improved quantitative microanalysis. In J.T. Armstrong, Ed., Microbeam Analysis, p. 104–106. San Francisco Press, California.

Redhammer, G.J. and Roth, G. (2002) Single-crystal structure refinements and crystal chemistry of synthetic trioctahedral micas $KM_3(Al^{3+}, Si^{4+})4O_{10}(OH)_2$, where M = Ni^{2+}, Mg^{2+}, Co^{2+}, Fe^{2+}, or Al^{3+}. American Mineralogist, 87, 1464-1476.

Redhammer, G.J., Amthauer, G., Lottermoser, W., Bernroider, M., Tippelt, G., and Roth, G. (2005) X-ray powder diffraction and ^{57}Fe-Mössbauer spectroscopy of synthetic trioctahedral micas $\{K\}[Me_3]<TSi_3>O_{10}(OH)_2$, Me = Ni^{2+}, Mg^{2+}, Co^{2+}, Fe^{2+}; T = Al^{3+}, Fe^{3+}. Mineralogy and Petrology, 85, 89-115.

Renner, B. and Lehmann, G. (1986) Correlation of angular and bond length distortions in TO4 units in crystals. Zeitschrift für Kristallographie, 175, 43–59.

Rittmann, A. (1962) Volcanoes and their activity. Wiley ed. New York, 305 p.

Robert, J-L., Beny, J-M., Della Ventura, G., and Hardy, M. (1993) Fluorine in micas: crystal-chemical control of the OH-F distribution between trioctahedral and dioctahedral sites. European Journal of Mineralogy, 5, 7–18.

Robinson, K., Gibbs, G.V., and Ribbe, P.H. (1971) Quadratic elongation: a quantitative measure of distortion in coordination polyhedra. Science, 172, 567–570.

Romano, R. (1982): Succession of the volcanic activity in the Etnean area. Mem Soc Geol It., 23, 27–48.

Russell, R.L. and Guggenheim, S. (1999) Crystal structure of near-end-member phlogopite at high temperature and heat treated Fe-rich phlogopite: the influence of the O, OH, F site. Canadian Mineralogist, 37, 711–720.

Schingaro, E., Mesto, E., Scordari, F., Brigatti, M.F., and Pedrazzi, G. (2005) Cation site partitioning in Ti-rich micas from Black Hill (Australia): A multi-technical approach. Clays and Clay Minerals, 53, 179–189.

538 Schingaro, E., Scordari, F., Matarrese, S., Mesto, E., Stoppa, F., Rosatelli, G., and Pedrazzi, G.
539 (2007) Phlogopite from the Ventaruolo subsynthem volcanics (Mt Vulture, Italy): a multi-method
540 study. Mineralogical Magazine, 71, 519–537.
541 Schingaro, E., Lacalamita, M., Scordari, F., Brigatti, M.F., and Pedrazzi, G. (2011) Crystal
542 chemistry of Ti-rich fluorophlogopite from Presidente Olegario, Alto Paranaíba igneous
543 province, Brazil. American Mineralogist, 96, 732-743.
544 Scordari, F., Ventruti, G., Sabato, A., Bellatreccia, F., Della Ventura, G., and Pedrazzi, G. (2006)
545 Ti-rich phlogopite from Mt. Vulture (Potenza, Italy) investigated by a multianalytical approach:
546 substitutional mechanisms and orientation of the OH dipoles. European Journal of Mineralogy,
547 18, 379–391.
548 Scordari, F., Schingaro, E., Ventruti, G., Lacalamita, M., and Ottolini, L. (2008) Red micas from
549 basal ignimbrites of Mt. Vulture (Italy): interlayer content appraisal by a multi-methodic
550 approach. Physics and Chemistry of Minerals, 35, 163–174.
551 Scordari, F., Dyar, M.D., Schingaro, E., Lacalamita, M., and Ottolini, L. (2010) XRD, micro-
552 XANES, EMPA, and SIMS investigation on phlogopite single crystals from Mt. Vulture (Italy).
553 American Mineralogist, 95, 1657–1670.
554 Shannon, R.D. (1976) Revised effective ionic radii and systematic studies of interatomic distances
555 in halides and chalcogenides. Acta Crystallographica, A32, 751–767.
556 Sheldrick, G.M. (2003) SADABS, Program for Empirical Absorption Correction of Area Detector
557 Data. University of Göttingen, Germany.
558 Stelling, J., Botcharnikov, R.E., Beermann, O., Nowak, M. (2008) Solubility of H2O- and chlorine-
559 bearing fluids in basaltic melt of Mount Etna at T=1050-1250°C and P=200 MPa. Chemical
560 Geology, 256, 102-110.
561 Takeda, H. and Donnay, J.D.H. (1966) Trioctahedral one-layer micas. III. Crystal structure of a
562 synthetic Lithium Fluormica. Acta Crystallographica, 20, 638–646.

Takeda, H. and Morosin, B. (1975) Comparison of observed and predicted structural parameters of mica at high temperature. Acta Crystallographica, B31, 2444–2452.

Toraya, H., Iwai, S., and Marumo, F. (1978) The crystal structure of synthetic mica, $KMg_{2.75}Si_{3.5}Al_{0.5}O_{10}F_2$. Mineralogical Journal, 9, 210–220.

Toraya, H. (1981) Distortions of octahedra and octahedral sheets in 1*M* micas and the relation to their stability. Zeitschrift für Kristallographie, 157, 173–190.

Toraya, H., Marumo, F., and Hirao, M. (1983) Synthesis and the crystal structure of a mangaoan fluoromica, $KMg_{2.14}Mn_{0.24}Si_{3.82}Mn_{0.18}O_{10}F_2$. Mineralogical Journal, 11, 240–247.

Ventruti, G., Zema, M., Scordari, F., and Pedrazzi, G. (2008) Thermal behavior of a Ti-rich phlogopite from Mt. Vulture (Potenza, Italy): An in situ X-ray single-crystal diffraction study. American Mineralogist, 93, 632–643.

Ventruti, G., Levy, D., Pavese, A., Scordari, F. and Suard E. (2009) High-temperature treatment, hydrogen behaviour and cation partitioning of a Fe–Ti bearing volcanic phlogopite by in situ neutron powder diffraction and FTIR spectroscopy, European journal of Mineralogy, 21, 385 – 396.

Viccaro, M. and Cristofolini, R. (2008) Nature of mantle heterogeneity and its role in the geochemical and volcanological evolution of Mt. Etna (Italy). Lithos, 105, 272–288.

Viccaro, M., Nicotra, E., Millar, I.L., Cristofolini, R. (2011) The magma source at Mount Etna volcano: perspectives from the Hf isotope composition of historic and recent lavas. Chemical Geology, 281, 343-351.

Waters, D.J. and Charnley, N.R. (2002) Local equilibrium in polymetamorphic gneiss and the titanium substitution in biotite. American Mineralogist, 87, 383–396.

Weiss, Z., Rieder, M., Chmielová, M., and Krajíček, J. (1985) Geometry of the octahedral coordination in micas: a review of refined structures. American Mineralogist, 70, 747–757.

587 Weiss, Z., Rieder, M., and Chmielová, M. (1992) Deformation of coordination polyhedra and their
588 sheets in phyllosilicates. European Journal of Mineralogy, 4, 665–682.

589

590

591 **Figure captions**

592 FIGURE 1 A) Geodynamic framework of Southern Italy with the main domains involved in active
593 tectonics; B) Digital Elevation Model of Mt. Etna volcano (from Monaco et al. 2011) with location
594 of the North-East and South Rift zones.

595 FIGURE 2 FT-IR spectrum of a single crystal of Concazze fluorophlogopite recorded in the 3900–
596 2600 cm^{-1} by transmission-method. In the inset a typical OH-absorption band of a phlogopite is
597 shown for comparison.

598 FIGURE 3. Relationship between the *c* parameter and the $F^- + O^{2-}$ content. Symbols: solid squares =
599 fluorophlogopites of this study; open circle = fluorophlogopite from Biancavilla (Gianfagna et al.
600 2007); triangle pointing upward = SA phlogopite characterized by Ti and Fe^{3+}-oxy substitutions
601 (Ventruti et al. 2009); triangle pointing downward = synthetic near end-member phlogopite
602 (Redhammer and Roth 2002); triangle with plus = F-free, Ti-rich oxyphlogopite (Cesare et al.
603 2003); triangle with cross = MA1_14 Ti-rich fluorophlogopites from Olegario (Schingaro et al.
604 2011); diamond = VUT 191_19 phlogopite (Matarrese et al. 2008); pentagon = VUT 187_1
605 phlogopite (Schingaro et al. 2007); hexagon with plus = VUT 187_18 phlogopite (Schingaro et al.
606 2007); solid hexagon = PG5_1 phlogopite (Scordari et al. 2010); star = IGNA_24 phlogopite
607 (Lacalamita et al. 2011); solid circle = VUT215_1 phlogopite (Lacalamita et al. 2011); square with
608 plus = fluorophlogopite (Joswig 1972); hexagon with cross = VUT215_8 phlogopite (Lacalamita et
609 al. 2011); square with vertical line = fluorophlogopite (Hazen and Burnham 1973); square with
610 horizontal line = synthetic fluorophlogopite (Takeda and Morosin 1975); hexagon = VUT001_2
611 phlogopite (Scordari et al. 2010). Solid lines: join end member phlogopite (Redhammer and Roth
612 2002) - end member fluorophlogopite (Takeda and Morosin 1975); join end member phlogopite
613 (Redhammer et al. 2005) - oxyphlogopite (Cesare et al. 2003)

614 FIGURE 4. Relationship between the interlayer separation (t_{int}) and the $F^- + O^{2-}$ content. Solid lines,
615 symbols and average e.s.d. values as in Figure 3

FIGURE 5. Off-center shift of the M2 cation ($shift_{M2}$) *vs*. Ti content. Symbols and average e.s.d. values as in Figure 3

FIGURE 6 O4-O4 bond length *vs*. the $O^{2-} + F^{-}$ content. Symbols as in Figure 3.

FIGURE 7 Tetrahedral volume *vs*. the ΔK-O distance. Symbols as in Figure 3.

FIGURE 8 Solid line represents linear relation between *c* parameter and mean interlayer cation radius after Hawthorne et al. 1999 ; circles: phlogopites with different interlayer content from Hawthorne et al. 1999; solid square symbol: Concazze fluorophlogopite.

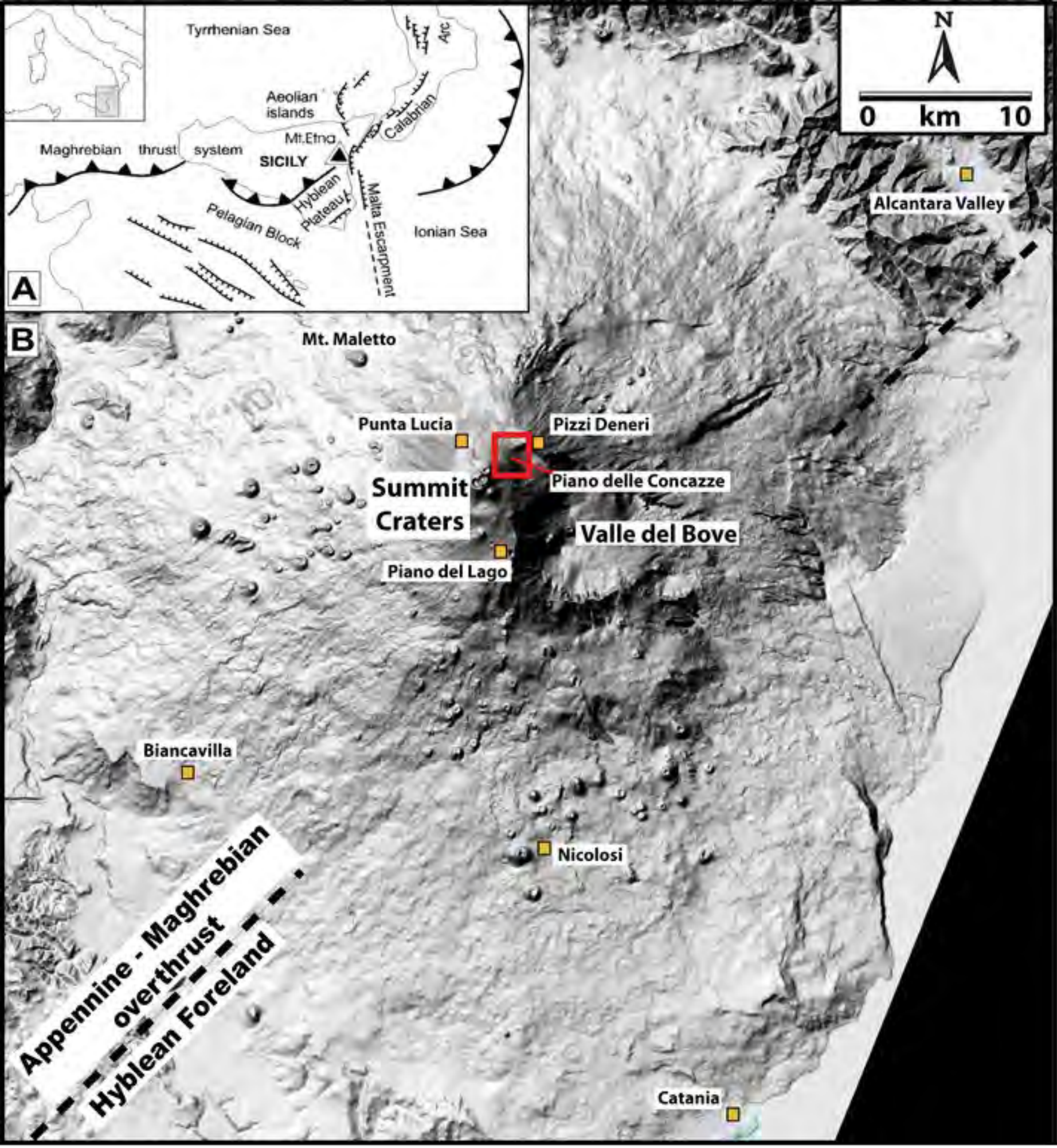
Tyrrhenian Sea
Arc
Aeolian islands
Calabrian
Mt.Etna
Maghrebian thrust system
SICILY
Hyblean Plateau
Malta Escarpment
Pelagian Block
Ionian Sea
A
B
N
0 km 10
Alcantara Valley
Mt. Maletto
Punta Lucia
Pizzi Deneri
Piano delle Concazze
Summit Craters
Valle del Bove
Piano del Lago
Biancavilla
Nicolosi
Catania
Appennine - Maghrebian overthrust
Hyblean Foreland

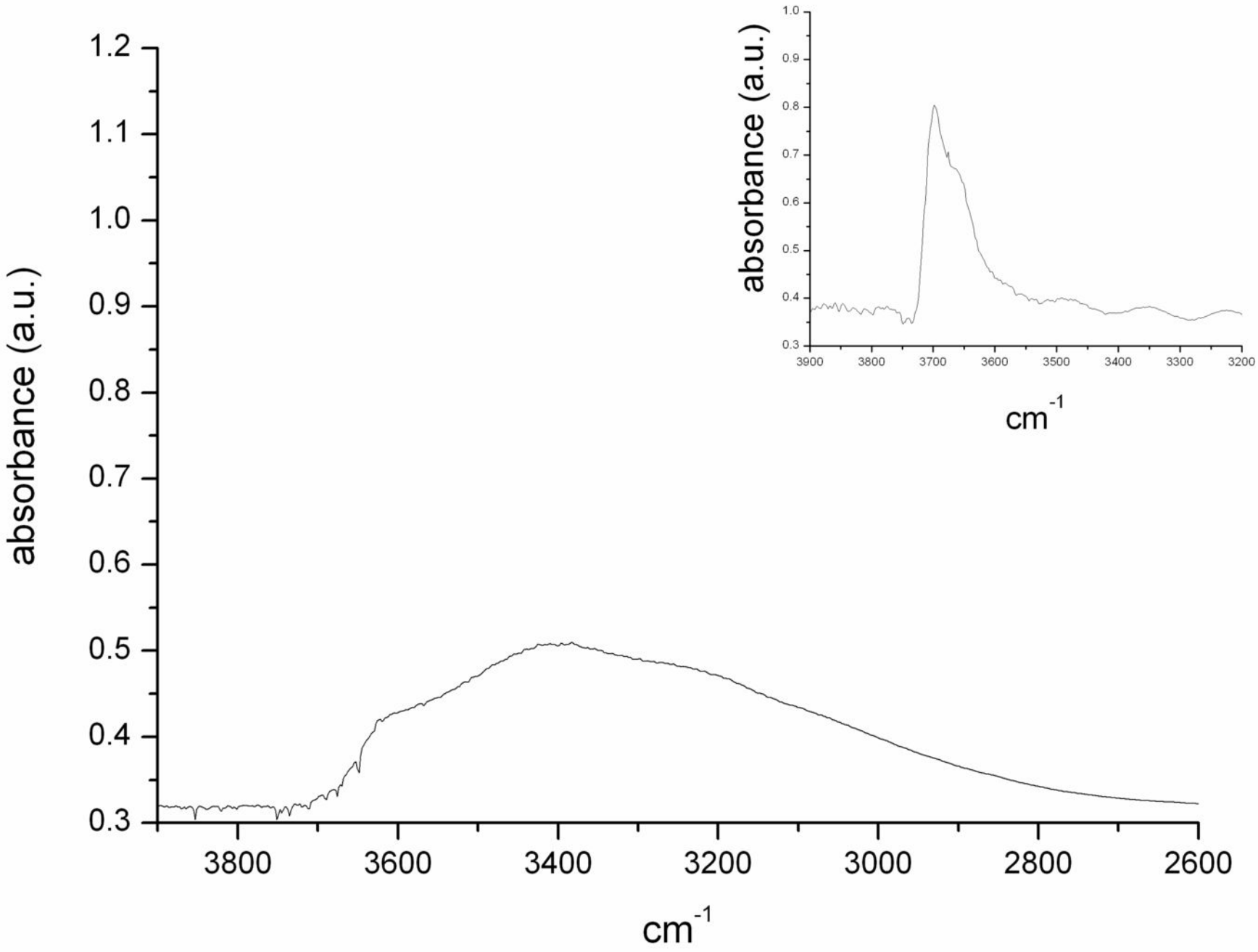
absorbance (a.u.)
1.2
1.1
1.0
0.9
0.8
0.7
0.6
0.5
0.4
0.3
3800
3600
3400
3200
3000
2800
2600
cm-1
absorbance (a.u.)
1.0
0.9
0.8
0.7
0.6
0.5
0.4
0.3
3900
3800
3700
3600
3500
3400
3300
3200
cm-1

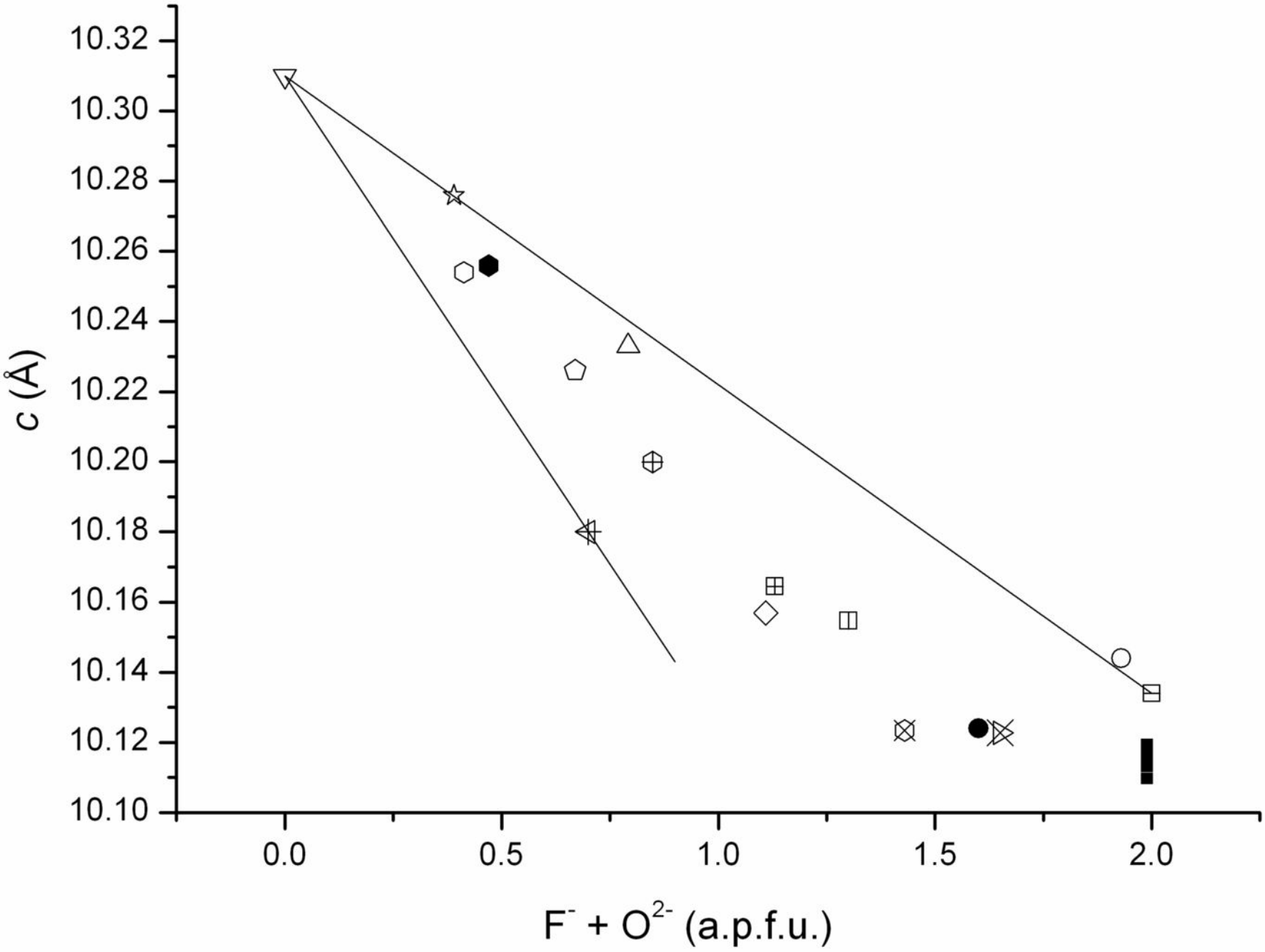
10.32
10.30
10.28
10.26
10.24
10.22
10.20
10.18
10.16
10.14
10.12
10.10
c (Å)
0.0
0.5
1.0
1.5
2.0
F- + O2- (a.p.f.u.)

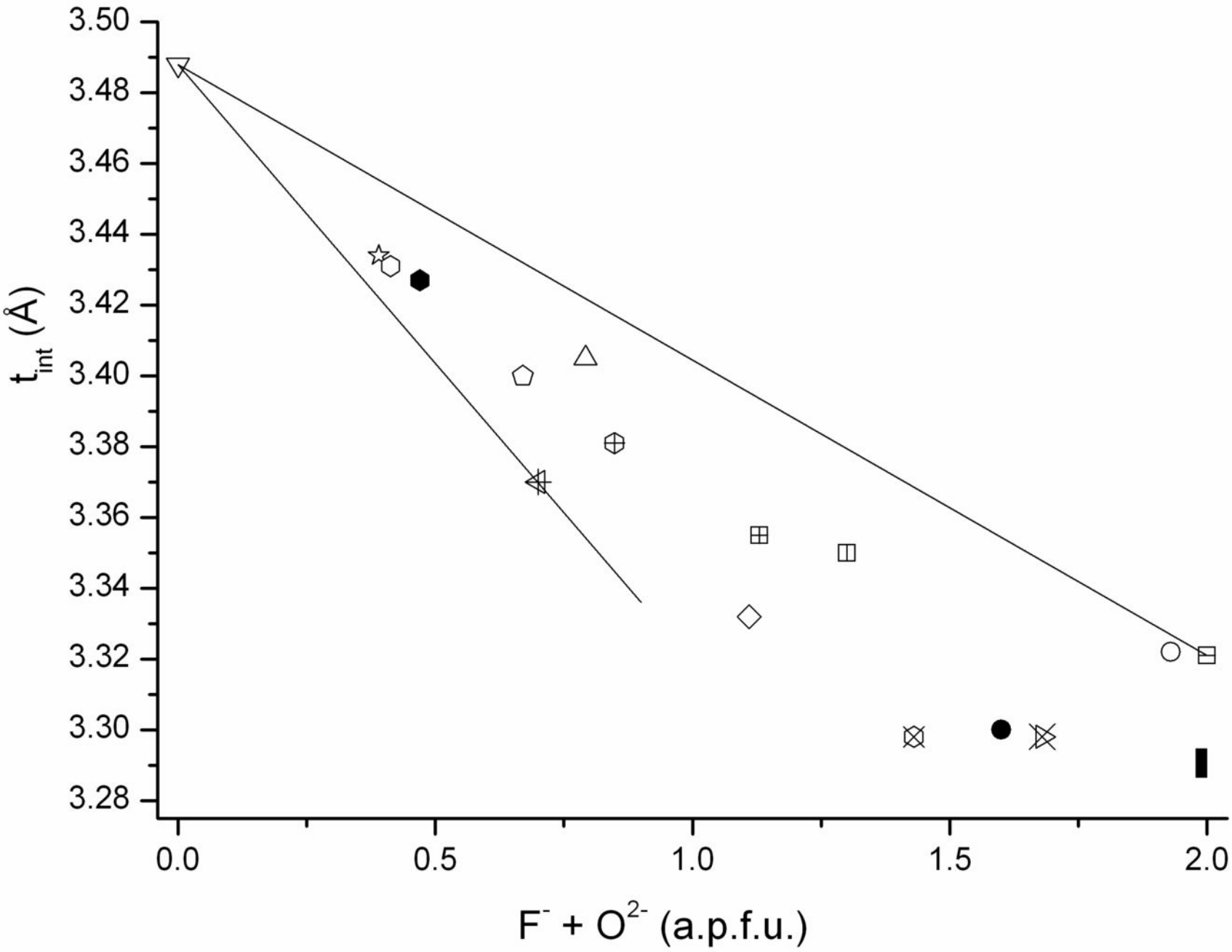
3.50
3.48
3.46
3.44
3.42
3.40
3.38
3.36
3.34
3.32
3.30
3.28
t_{int} (Å)
0.0
0.5
1.0
1.5
2.0
$F^- + O^{2-}$ (a.p.f.u.)

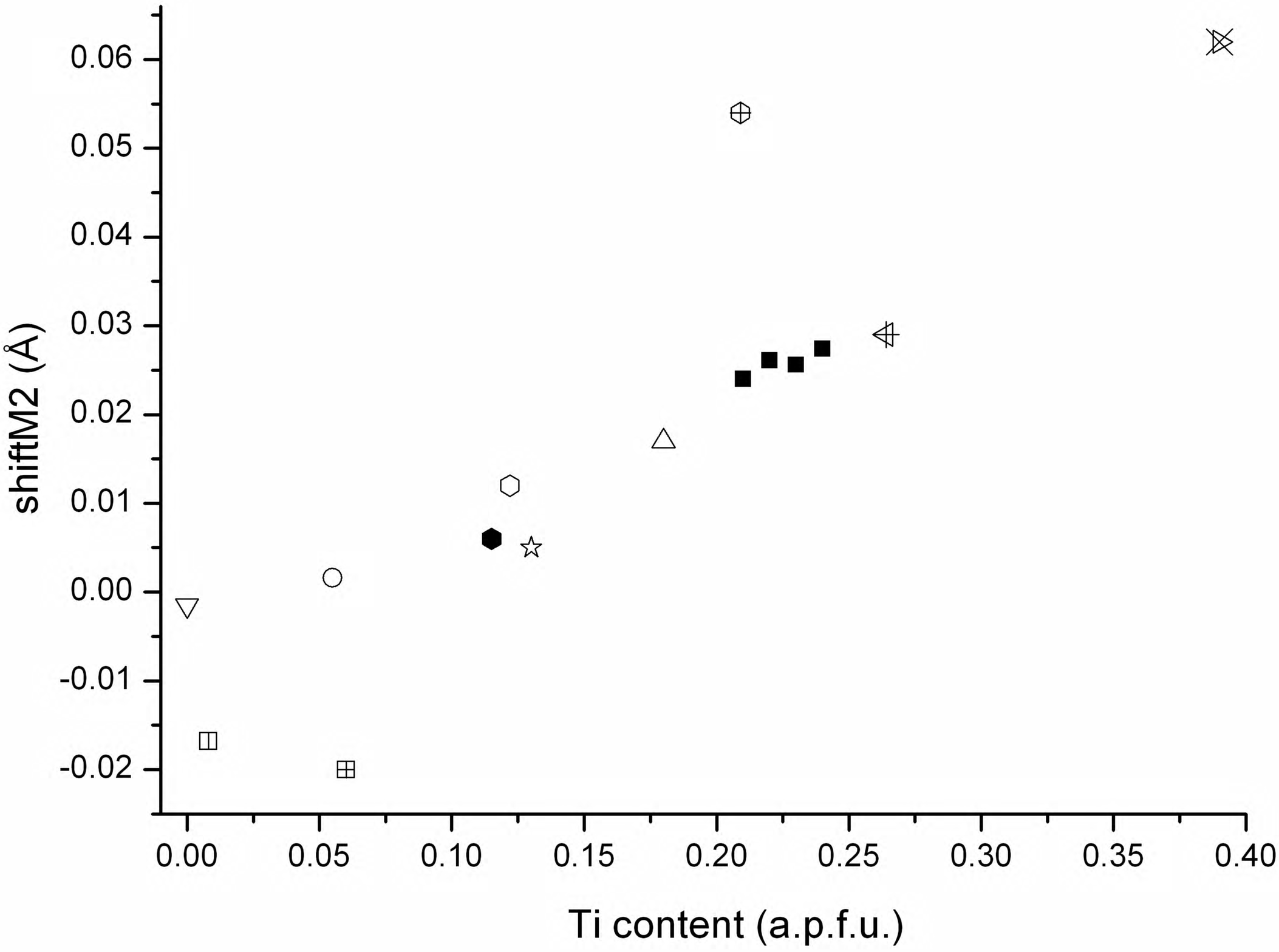
shiftM2 (Å)
0.06
0.05
0.04
0.03
0.02
0.01
0.00
-0.01
-0.02
0.00
0.05
0.10
0.15
0.20
0.25
0.30
0.35
0.40
Ti content (a.p.f.u.)

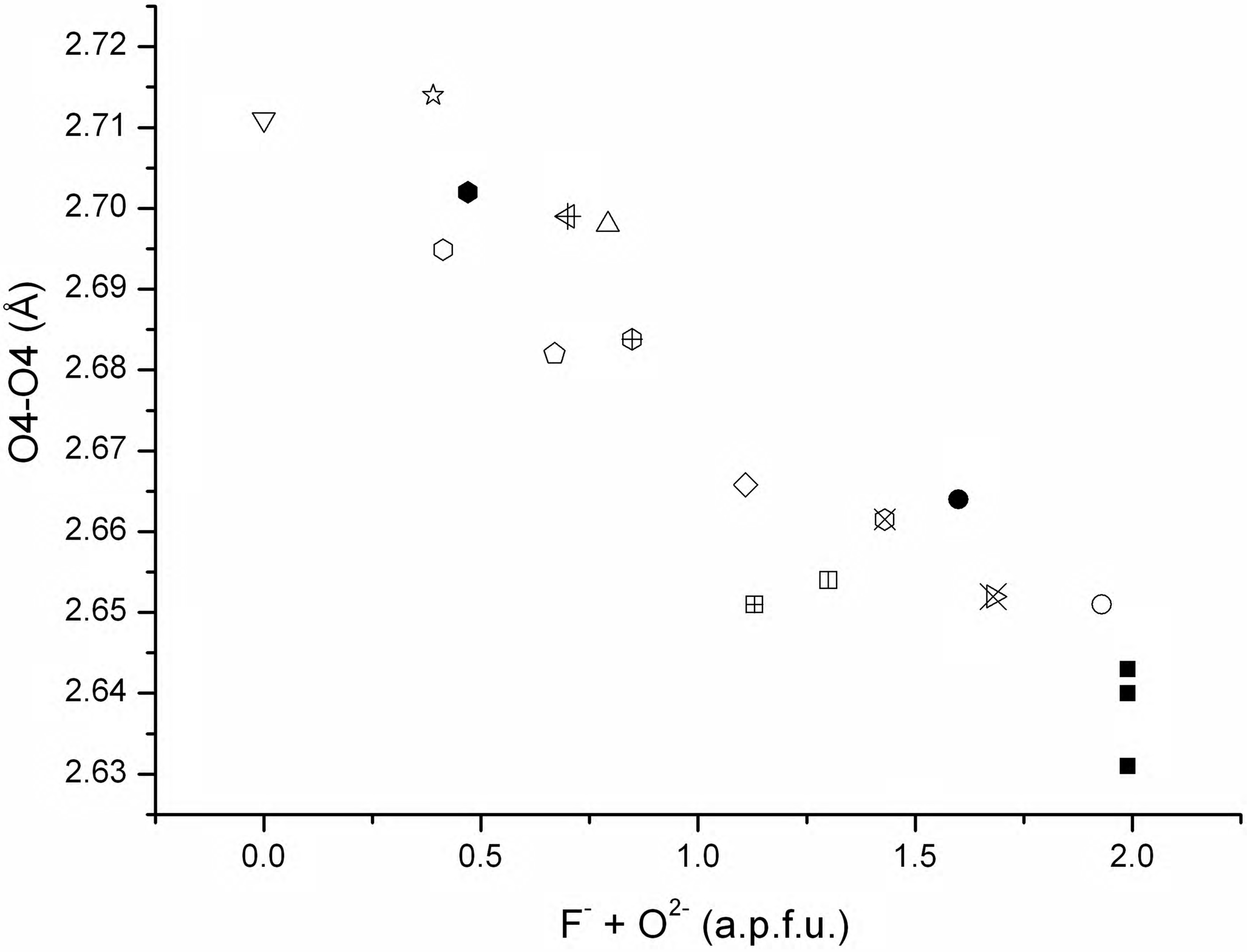
2.72
2.71
2.70
2.69
2.68
2.67
2.66
2.65
2.64
2.63
O4-O4 (Å)
0.0
0.5
1.0
1.5
2.0
F- + O2- (a.p.f.u.)

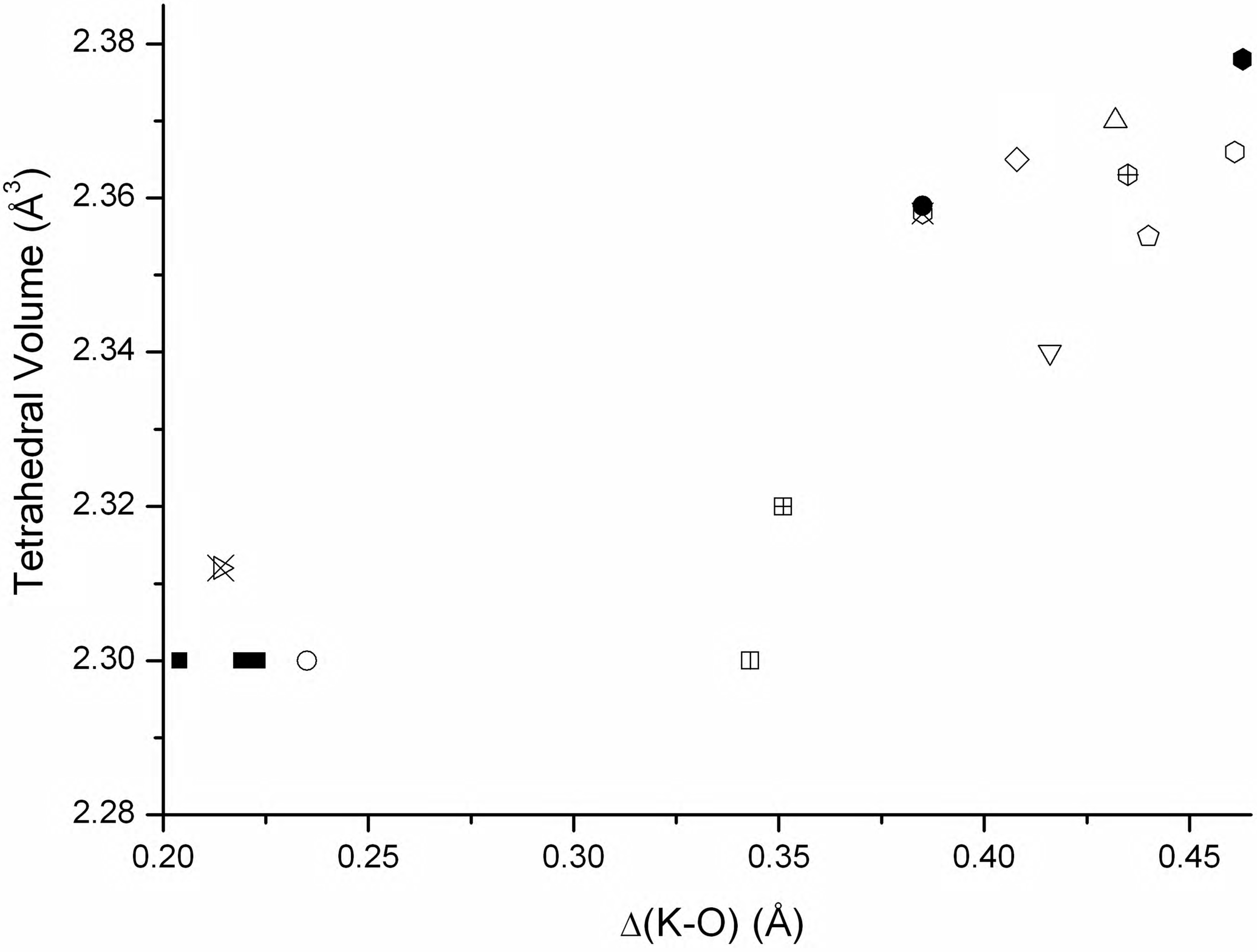
Tetrahedral Volume (Å^3)
2.38
2.36
2.34
2.32
2.30
2.28
0.20
0.25
0.30
0.35
0.40
0.45
Δ(K-O) (Å)

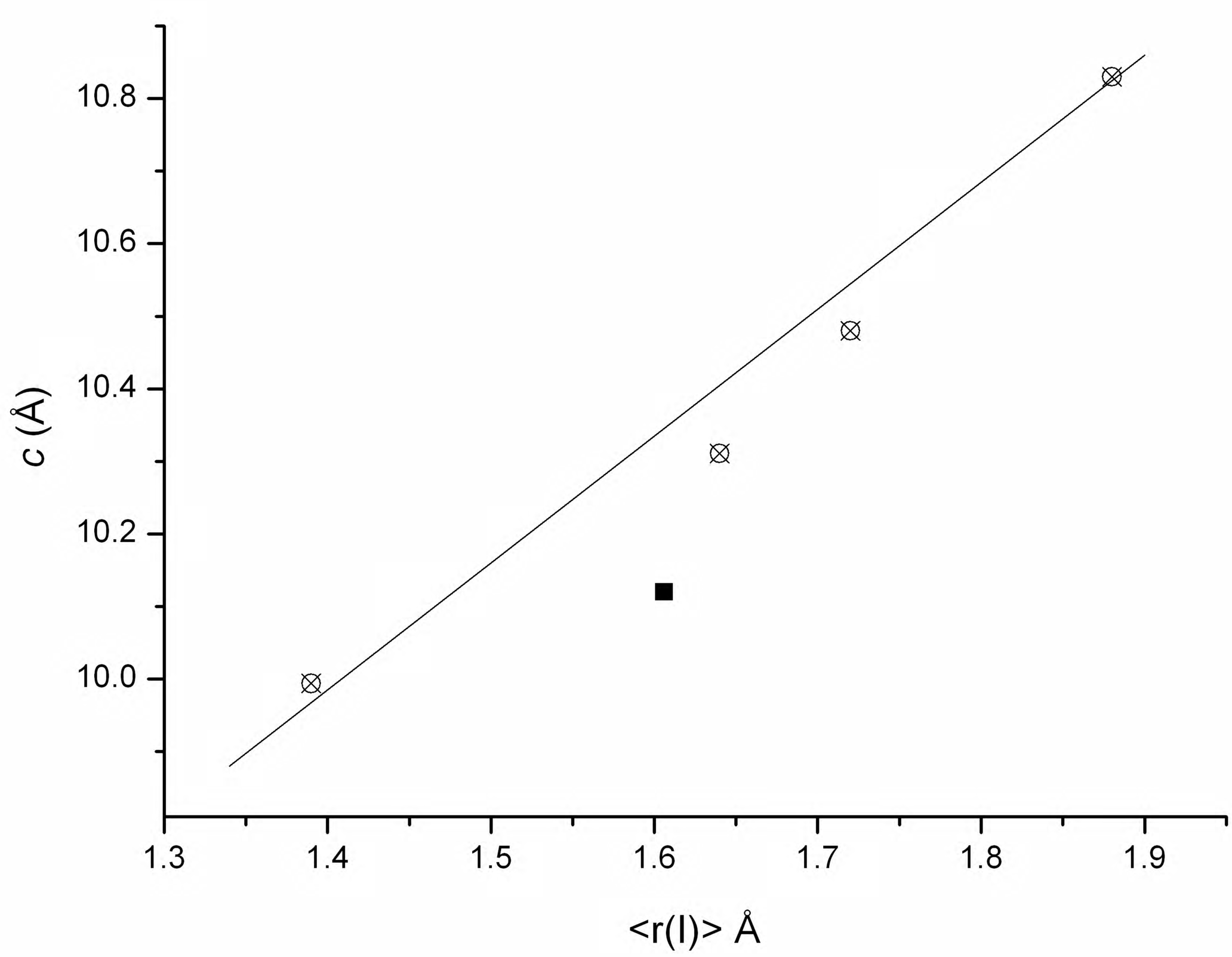
10.8
10.6
10.4
10.2
10.0
c (Å)
1.3
1.4
1.5
1.6
1.7
1.8
1.9
<r(l)> Å

TABLE 1. Chemical composition from EPMA and atomic proportion (a.p.f.u.) determined by combining, EPMP, Infrared and structural data.

oxide (wt %)	E0	E1	E2	E3
SiO_2	41.54(43)	41.00(25)	41.58(34)	42.26(34)
TiO_2	4.09(9)	4.29(13)	3.84(9)	3.96(13)
Al_2O_3	10.97(16)	11.03(14)	11.10(15)	11.18(12)
FeO_{tot}	8.21(17)	8.21(17)	9.06(33)	8.12(37)
MnO	0.13(4)	0.13(6)	0.15(4)	0.15(3)
MgO	20.12(32)	19.81(33)	19.55(23)	19.62(58)
BaO	0.05(4)	0.06(5)	0.03(1)	0.04(3)
CaO	-	0.01(1)	0.02(1)	0.01(1)
Na_2O	0.72(8)	0.92(5)	1.11(3)	0.82(20)
K_2O	9.10(18)	8.84(15)	8.52(8)	8.83(38)
F	6.04(17)	5.72(37)	5.59(12)	5.75(38)
Cl	0.09(1)	0.09(1)	0.07(1)	0.08(3)
H_2O^*	0.0	0.0	0.0	0.0
Total	101.01	100.11	100.62	100.82
a.p.f.u.				
Si	3.08(2)	3.04(3)	3.08(2)	3.13(2)
Al	0.92(2)	0.96(3)	0.92(2)	0.87(2)
Σ T	4.00	4.00	4.00	4.00
Al	0.03(2)	0.01(1)	0.05(2)	0.10(2)
Mg	2.22(3)	2.19(3)	2.16(2)	2.17(5)
Fe^{2+}	0.44(7)	0.39(8)	0.40(4)	0.46(6)
Fe^{3+}	0.07(7)	0.16(8)	0.16(4)	0.04(6)
Ti	0.23(1)	0.24(1)	0.22(1)	0.22(1)
Mn	0.01(0)	0.01(0)	0.01(0)	0.01(0)
Σ Oct.	3.00	3.00	3.00	3.00
K	0.86(1)	0.84(1)	0.81(1)	0.83(3)
Na	0.10(1)	0.13(1)	0.16(1)	0.12(3)
Ca	-	-	-	-
Ba	-	-	-	-
Σ Int.	0.96	0.97	0.97	0.95
OH^*	0.0	0.0	0.0	0.0
F	1.41(4)	1.34(8)	1.31(3)	1.35(8)
Cl	0.01(0)	0.01(0)	0.01(0)	0.01(0)
Σ A	1.42	1.35	1.32	1.36

Notes: *Estimated from FTIR analysis; T = Tetrahedral ; Oct. = Octahedral ; Int. = Interlayer; A = Anion

Table 2 Refined cell parameters and data-collection parameters for the samples studied by single-crystal XRD.

Sample name		E0	E1	E2	E3
Crystal dimensions (mm)		0.320- x 0.310- x 0.040	0.630 x 0.340 x 0.030	0.400 x 0.270 x 0.050	0.450 x 0.410 x 0.040
Crystal system		Monoclinic	Monoclinic	Monoclinic	Monoclinic
Space group		*C2/m*	*C2/m*	*C2/m*	*C2/m*
Unit-cell dimension	*a* (Å)	5.3192(3)	5.3239(3)	5.3200(2)	5.3237(2)
	b (Å)	9.2181(5)	9.2204(4)	9.2138(4)	9.2221(3)
	c (Å)	10.1096(6)	10.1192(5)	10.1130(4)	10.1159(3)
	β (°)	100.168(4)	100.185(3)	100.228(2)	100.249(2)
Volume ($Å^3$)		487.92(5)	488. 91(4)	487.84(3)	488.72(3)
θ range for data collection (°)		2 to 44.6	2 to 44.6	4 to 41.4	2 to 43.8
Index range		-10≤h≤10	-10≤h≤10	-9≤h≤9	-10≤h≤10
		0≤k≤17	0≤k≤17	-17≤k≤17	0≤k≤17
		0≤l≤19	0≤l≤19	-17≤l≤18	0≤l≤19
Reflections collected/ *R* merging [$R_{(int)}$] (%)		4265/6.93	4376/5.25	2919/2.43	4244/3.16
Reflections used		1686 with I>3σ(I)	2072 with I>3σ(I)	1250 with I>3σ(I)	2127 with I>3σ(I)
No. of refined parameters		71	71	68	71
Goof[a]		0.77	0.72	0.57	0.70
R_1[b] (on *F*)/ wR_2[b] (on F^2)		0.0385/0.0415	0.0315/0.0324	0.0296/0.0304	0.0267/0.0258
$(\Delta/\sigma)_{max}$		0.016	0.014	0.014	0.014
$\Delta\rho_{min}$/ $\Delta\rho_{max}$(e/$Å^3$)		-1.81/2.39	-1.89/0.66	-0.62/0.71	-0.55/0.58

Table 3 Crystallographic coordinates and displacement parameters of the studied micas. In square brackets are quoted the cations used for occupancy refinement

Atom	x/a	y/b	z/c	Occupancy	U_{iso}	U_{11}	U_{22}	U_{33}	U_{12}	U_{13}	U_{23}
Sample	E0										
K	0	0	0	0.9049(9)	0.0318	0.0331(10)	0.0300(6)	0.0325(6)	0	0.0059(7)	0
T[Si]	0.5745(1)	0.16681(5)	0.22369(5)	0.9861(10)	0.0092	0.0086(3)	0.0074(2)	0.0119(2)	0.0001(2)	0.0026(2)	0.0002(2)
M1[Mg]	0	0.5	0.5	0.7726(8)	0.0098	0.0088(6)	0.0060(3)	0.0154(4)	0	0.0042(4)	0
M1[Fe]	0	0.5	0.5	0.2277(7)	0.0098	0.0088(6)	0.0060(3)	0.0154(4)	0	0.0042(4)	0
M2[Mg]	0	0.83604(9)	0.5	0.8113(8)	0.0105	0.0074(4)	0.0119(3)	0.0125(3)	0	0.0025(3)	0
M2[Fe]	0	0.83604(9)	0.5	0.1889(7)	0.0105	0.0074(4)	0.0119(3)	0.0125(3)	0	0.0025(3)	0
O1	0.8176(4)	0.2381(2)	0.1652(2)	1.0000(8)	0.0183	0.0162(10)	0.0225(7)	0.0165(6)	-0.0011(5)	0.0038(7)	-0.0064(6)
O2	0.5302(6)	0	0.1655(2)	1.0000(8)	0.0186	0.028(2)	0.0119(7)	0.0153(8)	0	0.0012 (9)	0
O3	0.6304(3)	0.1675(2)	0.3898(1)	1.0000(8)	0.0100	0.0097(7)	0.0084(4)	0.0125(4)	-0.0001(4)	0.0035(5)	0.0005(5)
F4	0.1306(5)	0	0.4003(2)	1.0000(8)	0.0129	0.0129(11)	0.0118(6)	0.0147(7)	0	0.0044(8)	0
Sample	E1										
K	0	0	0	0.9131(7)	0.0314	0.0314(4)	0.0313(5)	0.0308(4)	0	0.0042(3)	0
T[Si]	0.57457(6)	0.16688(4)	0.22366(4)	0.9819(9)	0.0089	0.0079(1)	0.0083(1)	0.0103(1)	0.0000(1)	0.0011(1)	0.0000(1)
M1[Mg]	0	0.5	0.5	0.7762(8)	0.0094	0.0077(2)	0.0070(2)	0.0136(3)	0	0.0024(2)	0
M1[Fe]	0	0.5	0.5	0.2236(6)	0.0094	0.0077(2)	0.0070(2)	0.0136(3)	0	0.0024(2)	0
M2[Mg]	0	0.83630(6)	0.5	0.8019(8)	0.0108	0.0066(2)	0.0138(2)	0.0118(2)	0	0.0007(1)	0
M2[Fe]	0	0.83630(6)	0.5	0.1980(7)	0.0108	0.0066(2)	0.0138(2)	0.0118(2)	0	0.0007(1)	0
O1	0.8170(2)	0.2377(1)	0.1651(1)	1.0000(8)	0.0177	0.0160(4)	0.0231(5)	0.0139(4)	-0.0015(3)	0.0027(3)	-0.0060(4)
O2	0.5303(3)	0	0.1657(2)	1.0000(8)	0.0179	0.0260(7)	0.0126(5)	0.0139(6)	0	0.0003(5)	0
O3	0.6307(2)	0.1676(1)	0.38978(9)	1.0000(8)	0.0103	0.0097(3)	0.0102(3)	0.0107(3)	-0.0002(3)	0.0013(2)	0.0004(3)
F4	0.1298(2)	0	0.4008(1)	1.0000(8)	0.0128	0.0108(4)	0.0142(5)	0.0134(5)	0	0.0019(4)	0

.

Atom	x/a	y/b	z/c	Occupancy	U_{iso}	U_{11}	U_{22}	U_{33}	U_{12}	U_{13}	U_{23}
Sample	E2										
K	0	0	0	0.8939(8)	0.0316	0.0317(5)	0.0311(5)	0.0319(5)	0	0.0052(4)	0
T[Si]	0.57444(7)	0.16685(4)	0.22370(4)	0.9862(9)	0.0088	0.0086(1)	0.0076(1)	0.0104(2)	0.0000(1)	0.0020(1)	0.0001(1)
M1[Mg]	0	0.5	0.5	0.7759(8)	0.0092	0.0083(3)	0.0062(3)	0.0138(3)	0	0.0036(2)	0
M1[Fe]	0	0.5	0.5	0.2237(6)	0.0092	0.0083(3)	0.0062(3)	0.0138(3)	0	0.0036(2)	0
M2[Mg]	0	0.83595(7)	0.5	0.8068(8)	0.0104	0.0069(2)	0.0126(2)	0.0120(2)	0	0.0020(2)	0
M2[Fe]	0	0.83595(7)	0.5	0.1932(7)	0.0104	0.0069(2)	0.0126(2)	0.0120(2)	0	0.0020(2)	0
O1	0.8166(2)	0.2379(2)	0.1650(1)	1.0000(8)	0.0181	0.0167(5)	0.0227(6)	0.0151(5)	-0.0014(4)	0.0037(4)	-0.0059(4)
O2	0.5304(4)	0	0.1655(2)	1.0000(8)	0.0182	0.0261(8)	0.0132(6)	0.0145(7)	0	0.0014 (6)	0
O3	0.6308(2)	0.1673(1)	0.3899(1)	1.0000(8)	0.0095	0.0088(3)	0.0085(3)	0.0114(4)	-0.0003(3)	0.0024(3)	0.0004(3)
F4	0.1307(3)	0	0.4004(2)	1.0009(8)	0.0130	0.0111(5)	0.0140(6)	0.0144(6)	0	0.0034(4)	0
Sample	E3										
K	0	0	0	0.8970(7)	0.0311	0.0318(3)	0.0312(4)	0.0299(3)	0	0.0048(3)	0
T[Si]	0.57472(5)	0.16681(3)	0.22370(3)	0.9808(9)	0.0090	0.0088(1)	0.0083(1)	0.0099(1)	0.0000(1)	0.0017(1)	0.0001(1)
M1[Mg]	0	0.5	0.5	0.7672(7)	0.0098	0.0087(2)	0.0078(2)	0.0135(2)	0	0.0032(1)	0
M1[Fe]	0	0.5	0.5	0.2323(6)	0.0098	0.0087(2)	0.0078(2)	0.0135(2)	0	0.0032(1)	0
M2[Mg]	0	0.83616(5)	0.5	0.7932(7)	0.0111	0.0077(1)	0.0140(2)	0.0115(1)	0	0.0014(1)	0
M2[Mg]	0	0.83616(5)	0.5	0.2065(6)	0.0111	0.0077(1)	0.0140(2)	0.0115(1)	0	0.0014(1)	0
O1	0.8170(2)	0.2379(1)	0.16507(8)	1.0000(8)	0.0187	0.0173(3)	0.0244(4)	0.0145(3)	-0.0016(3)	0.0032(2)	-0.0069(3)
O2	0.5306(3)	0	0.1658(1)	1.0000(8)	0.0183	0.0272(6)	0.0128(4)	0.0139(4)	0	0.0012(4)	0
O3	0.6309(1)	0.16750(8)	0.38995(7)	1.0000(8)	0.0104	0.0105(2)	0.0104(2)	0.0102(4)	0.0001(2)	0.0016(2)	0.0005(2)
F4	0.1302(2)	0	0.4005(1)	1.0008(7)	0.0129	0.0119(3)	0.0142(4)	0.0127(3)	0	0.0023(3)	0

Table 4 Selected bond distances (Å). Standard deviations are given in parentheses.

	E0	E1	E2	E3
T-O1	1.650(2)	1.647(1)	1.647(1)	1.6482(9)
T-O1'	1.644(2)	1.649(1)	1.648(1)	1.6486(9)
T-O2	1.648(1)	1.6488(7)	1.6479(7)	1.6480(5)
T-O3	1.653(2)	1.655(1)	1.654(1)	1.6550(7)
<T-O>	1.649(2)	1.650(1)	1.649(1)	1.6500(8)
M1-O4(x2)	2.044(3)	2.047(1)	2.042(1)	2.046(1)
M1-O3(x4)	2.093(1)	2.0951(9)	2.092(1)	2.0944(7)
<M1-O>	2.077(2)	2.079(1)	2.075(1)	2.078(1)
M2-O4(x2)	2.008(2)	2.002(1)	2.008(1)	2.0064(7)
M2-O3(x2)	2.082(2)	2.0820(9)	2.079(1)	2.0795(7)
M2-O3'(x2)	2.100(2)	2.103(1)	2.101(1)	2.1023(8)
<M2-O>	2.063(2)	2.062(1)	2.063(1)	2.0627(7)
<M-O>	2.068(2)	2.068(1)	2.067(1)	2.068(1)
K-O1(x4)	3.020(2)	3.020(1)	3.020(1)	3.021(1)
K-O1'(x4)	3.237(2)	3.239(1)	3.233(1)	3.237(1)
K-O2 (x2)	3.015(3)	3.018(2)	3.015(2)	3.018(1)
K-O2'(x2)	3.244(3)	3.248(2)	3.244(2)	3.248(1)
$<K\text{-}O>_{inner}$	3.018(2)	3.019(1)	3.018(1)	3.020(1)
$<K\text{-}O>_{outer}$	3.239(2)	3.242(1)	3.237(1)	3.241(1)
<K-O>	3.129(2)	3.131(1)	3.128(1)	3.131(1)

Table 5 Selected distortion parameters of the studied crystals.

	E0	E1	E2	E3
t_{tet} [Å]	2.234	2.236	2.237	2.236
BLD $_T$	0.177	0.134	0.149	0.165
Volume $_T$ [Å^3]	2.30	2.30	2.30	2.30
TQE	1.0005	1.0005	1.0005	1.0005
TAV	1.944	1.948	2.077	1.887
τ [°]	110.66	110.66	110.71	110.64
α [°]	4.83	4.87	4.80	4.81
Δz [Å]	0.003	0.006	0.005	0.007
D.M. [Å]	0.477	0.480	0.478	0.482
Ψ_{M1} [°]	59.25	59.32	59.26	59.32
Ψ_{M2} [°]	59.03	59.04	59.04	59.07
BLD_{M1}	1.043	1.020	1.054	1.044
ELD_{M1}	5.412	5.495	5.423	5.502
BLD_{M2}	1.785	1.945	1.779	1.828
ELD_{M2}	5.153	5.167	5.175	5.202
$Shift_{M2}$ [Å]	0.0250	0.0274	0.0240	0.0261
Volume $_{M1}$ [Å]	11.71	11.75	11.68	11.72
OQE_{M1}	1.013	1.014	1.013	1.014
OAV_{M1}	42.616	44.107	43.018	44.219
Volume $_{M2}$ [Å^3]	11.50	11.49	11.49	11.49
OQE_{M2}	1.012	1.012	1.012	1.013
OAV_{M2}	39.242	39.598	39.476	39.938
e_uM1/ e_sM1	1.114	1.116	1.115	1.117
e_uM2/ e_sM2	1.109	1.109	1.109	1.110
t_{oct} [Å]	2.124	2.122	2.122	2.120
t_{int} [Å]	3.290	3.293	3.288	3.292
Δ_{K-O} [Å]	0.221	0.223	0.219	0.221
t_{K-O4} [Å]	3.920	3.929	3.922	3.923

Note: t_{tet}: tetrahedral sheet thickness calculated from z coordinates of basal and apical O atoms; TQE: tetrahedral quadratic elongation calculated as TQE = $\sum_i(l_i/l_0)^2/4$ where l_0 is the center to vertex distance for an undistorted tetrahedron (Robinson et al. 1971); TAV: tetrahedral angle variance defined as TAV = $\sum_i(\theta_i\text{-}109.47°)^2/5$ (Robinson et al. 1971); τ: tetrahedral flattening angle; α: tetrahedral rotation angle (Hazen and Burnham, 1973); Δz: departure from co planarity of the basal O atoms, calculated as $\Delta z = (z_{o2} - z_{o1})c\sin\beta$ (Güven 1971); D.M.: dimensional misfit between tetrahedral and octahedral sheets defined as D.M. = [$2\sqrt{3}$ <O – O > $_{bas}$ - $3\sqrt{2}$ <M – O>] (Toraya 1981); Ψ: octahedral flattening angles (Donnay et al. 1964); BLD: bond-length distortions calculated as BLD = 100/n * $\sum_i$ I(M – O)$_i$ -<M – O> I / <M – O> (Renner and Lehmann 1986); ELD: edge-length distortion defined as ELD = 100/n * $\sum_i$ I(O – O)$_i$ -<O – O> I / <O – O>) (Renner and Lehman 1986); $Shift_{M2}$: off-center shift of the M2 cation defined as the distance between the refined position of cation and the geometrical center of M2 site (coordinates: x/a = 0.0, y/b = 0.8333, z/c = 0.5); OQE: octahedral quadratic elongation calculated as OQE = $\sum_i(l_i/l_0)^2/6$ where l_0 is the center to vertex distance for an undistorted octahedron (Robinson et al. 1971); OAV: octahedral angle variance defined as OAV = $\sum_i(\theta_i\text{-}90°)^2/11$ (Robinson et al. 1971); e_u,e_s: mean lengths of unshared and shared edges (Toraya 1981), respectively; t_{oct}: octahedral sheet thickness (Toraya, 1981); t_{int} calculated from the z coordinates of basal O atoms; Δ_{K-O} = <K-O>$_{outer}$-<K-O>$_{inner}$; t_{K-O4}: projection of K-O4 distance along c*

Table 6 Octahedral cation distribution, mean atomic numbers (m.a.n.s, e^-) of cation sites, octahedral and tetrahedral mean distances, as determined by structure refinement (Xref) and chemical determinations (EMPA). See text for details.

	E0	E1	E2	E3
$e^-_{(M1+M2)X\text{-}ref}$	44.49(3)	44.67(3)	44.53(3)	45.02(2)
$e^-_{(M1+M2)\ EMPA}$	45.60	46.24	46.22	45.43
K $e^-_{X\text{-}ref}$	17.19(2)	17.35(2)	16.98(2)	17.04(1)
K e^-_{EMPA}	17.44	17.39	17.15	17.09
T $e^-_{X\text{-}ref}$	13.81(1)	13.75(1)	13.81(1)	13.73(1)
T e^-_{EMPA}	13.77	13.76	13.77	13.78
Σ^+	22.60	22.66	22.70	22.66
Σ^-	22.58	22.65	22.68	22.64
$\langle T\text{-}O\rangle_{X\text{-}ref}$	1.649(2)	1.650(1)	1.649(1)	1.650(1)
$\langle T\text{-}O\rangle_{EMPA}$	1.655	1.655	1.655	1.654
$\langle M\text{-}O\rangle_{X\text{-}ref}$	2.068(2)	2.068(1)	2.067(1)	2.068(1)
$\langle M\text{-}O\rangle_{EMPA}$	2.067	2.065	2.064	2.063

Table 7 Selected structural parameters of Biancavilla and Olegario fluorphlogopites.

	Biancavilla	Olegario	This study
a	5.3094(4)	5.3275(3)	5.3217(3)
b	9.1933(7)	9.2278(3)	9.2186(4)
c	10.1437(8)	10.1334(2)	10.1144(5)
β	100.062(5)	100.183(3)	100.208(3)
t_{tet} [Å]	2.239	2.242	2.236
<T-O>	1.648(2)	1.652(1)	1.650(1)
Volume $_T$ [Å^3]	2.30	2.31	2.30
τ [°]	110.89	110.8	110.7
α [°]	5.17	4.68	4.83
Δz [Å]	0.003	0.011	0.005
Ψ_{M1} [°]	59.20	59.33	59.29
Ψ_{M2} [°]	59.16	59.03	59.05
<M1-O>	2.064(2)	2.082(1)	2.077(1)
<M2-O>	2.061(2)	2.064(1)	2.063(1)
$Shift_{M2}$ [Å]	0.0016	0.062	0.0256
Volume $_{M1}$ [Å]	11.49	11.79	11.72
Volume $_{M2}$ [Å^3]	11.44	11.51	11.49
toct [Å]	2.113	2.124	2.122
tint [Å]	3.322	3.298	3.291
Δ_{K-O} [Å]	0.235	0.214	0.221

Note: symbols as in Tab.5